Chemistry–A European Journal

Supporting Information

The Importance of Mg^{2+}-Free State in Nucleotide Exchange of Oncogenic K-Ras Mutants

Gyula Pálfy, Dóra K. Menyhárd, Hanna Ákontz-Kiss, István Vida, Gyula Batta, Orsolya Tőke, and András Perczel*

Resonance Assignment and Fast dynamics of GDP- and GTP-bound G12V K-Ras·Mg^{2+}

We have previously carried out the backbone resonance assignment of GDP- and GTP-bound wt, G12C, and G12D K-Ras·Mg^{2+} as well as that of GDP-bound G12V K-Ras·Mg^{2+}.[1,2] To complete these data, we determined the resonance assignment of G12V K-Ras·Mg^{2+}·GTP (Fig. S2). Resonance assignment of the GTP-bound form was accomplished based on the assignment of GTP-bound K-Ras-wt, G12C, and G12D mutants[2] complemented by 3D ^{15}N NOESY-HSQC measurements. Similarly to the other three variants, ~79% of non-proline residues were successfully assigned (Fig. S2). Unassigned residues are mostly found in switch-I (D30, E31, D33, I36-D38) and switch-II (D54-R73) regions and as reported earlier,[3] can likely be attributed to signal broadening arising from intrinsic conformational exchange on intermediate timescales.

To characterize the ps-ns dynamics of G12V K-Ras·Mg^{2+} and compare it with the previously investigated wild-type form and the G12C and G12D variants,[2] ^{15}N R_1, R_2, and ^{15}N-{^1H} HetNOE parameters were analyzed using the Lipari-Szabo model-free formalism and reduced spectral density mapping. General trends of both the GDP- and GTP-bound forms of G12V are similar to the other variants (Fig. S3, Table S1). Notably, the relaxation parameters have larger standard deviations in the GTP-bound form indicating that GTP-bound G12V K-Ras is dynamically more heterogeneous than its GDP-bound state. The GTP-bound form showed the largest average R_2/R_1 ratio and global correlation time (τ_c) among the investigated variants (12.8 ns *vs.* 12.0-12.6 ns for the others).

Parameters derived from Lipari-Szabo model-free analysis (S^2, R_{ex}, τ_e) and reduced spectral density mapping ($J(0)$, $J(\omega_N)$, $J(\omega_h)$) of the G12V mutant are in the same range and exhibit similar trends as the three other variants in both the GDP- and the GTP-bound states. Differences in the GDP-bound state in comparison to wt include a slight increase in S^2 in L3 (G48, T50), at the end of α3 (I100, K104), as well as in the mobile loop between β5 and α4 (L120, S122, V126, T127). The observed rigidification near the C-terminal end of α3 is similar to that found in G12C but differs markedly from G12D. An additional difference between G12V and the two other investigated mutants is observed in the switch-II region (E62) and in the middle of α3 (I93). While in G12C and G12D a significant rigidification is observed at these positions, the valine mutant exhibits a slight decrease in S^2. Moreover, unlike in G12D, where the switch-I region displays a decrease in ps-ns flexibility, G12V behaves similar to wt. However, together with the P-loop, positions in β2 and β3 (*e.g.* Q43, I46, D54, A56), the L79-V81 segment of β4, and two proximate segments of the allosteric lobe (L113-D119, S145-K147), the switch-I region exhibits a contribution from µs-ms motions, which appears to be more pronounced than in wt or the two other mutants. Among the affected residues in switch-I, similarly to the other investigated variants, E37 has the largest R_2 and R_{ex} values in the entire protein (23.35 s^{-1} and 7.04 s^{-1}, respectively). Motions of Y32 and D38 are more complex with contribution from both fast (τ_e) and slow (R_{ex}) motions. Similar to our investigation of wt, G12C, and G12D,[2] Y32 has an extremely low HetNOE (0.39 *vs.* switch-I average of 0.77) and high $J(\omega_H)$ (9.54 ps rad^{-1} *vs.* switch-I average of 3.37 ps rad^{-1}) value in GDP-bound G12V as well highlighting its flexibility in contrast to the surrounding switch-I residues. Remarkably, in the GTP-bound state it becomes rigid, characterized by increased HetNOE (0.91) and decreased $J(\omega_H)$ (1.11 ps rad^{-1}) values. The significant difference in the mobility of Y32 between the GDP- and GTP-bound forms of G12V is consistent with our suggestion for its role in GTP-autohydrolysis.[2] Unfortunately, severe line broadening obscures the analysis in most of switch-I and nearly the entire switch-II in the GTP-bound state. Motions on the ps-ns timescale in the rest of the protein are highly similar to wt and the two other variants. This includes a pronounced contribution of fast local motions in L7 (D105-V109) as well as in the L8/α4-region (S122-Q129). Regarding the P-loop, unlike in the GDP-bound form, no significant contribution from slow motions is indicated by model-free. While G13 shows a contribution from ps motions, dynamics of the rest of the P-loop can be described by S^2 alone.

Supplementary tables

Table S1. Averaged relaxation parameters determined for K-Ras-G12V in its nucleotide- and cofactor-bound forms as well as for Mg^{2+}-free K-Ras-G12C-GDP. Additional dynamic properties derived from the Lipari–Szabo model-free and reduced spectral density analysis (global correlation time, τ_c; generalized order parameter, S^2; spectral density function of fast motions, $J(\omega_h)$) are listed.

	K-Ras-G12V·Mg^{2+}·GTP		K-Ras-G12V·Mg^{2+}·GDP		Mg^{2+}-free K-Ras-G12C·GDP	
	average	min. → max.	average	min. → max.	average	min. → max.
R_1 / s^{-1}	0.80 ± 0.07	0.67 → 1.25	0.90 ± 0.06	0.82 → 1.13	0.96 ± 0.08	0.84 → 1.26
R_2 / s^{-1}	17.83 ± 2.90	5.65 → 24.78	15.97 ± 2.05	8.14 → 23.35	14.09 ± 2.03	5.90 → 22.87
R_2 / R_1	22.54 ± 4.29	4.51 → 31.50	17.77 ± 2.51	8.82 → 24.73	14.80 ± 2.47	4.77 → 20.32
HetNOE	0.76 ± 0.13	0.05 → 0.91	0.79 ± 0.10	0.38 → 0.91	0.77 ± 0.12	0.05 → 0.92
τ_c / ns	12.81	-	11.14	-	10.40	-
S^2	0.84 ± 0.08	0.52 → 0.99	0.85 ± 0.06	0.52 → 0.93	0.82 ± 0.09	0.49 → 1
$J(\omega_h)$ / ps rad^{-1}	3.13 ± 2.21	1.11 → 16.78	2.98 ± 1.82	0.94 → 16.99	3.60± 2.26	1.13 → 18.35

Table S2 Experimental fast dynamics parameters (R_1, R_2, R_2/R_1 and ^{15}N-{^1H} HetNOE) of K-Ras-G12V·Mg^{2+} bound to GTP and GDP recorded at 700 MHz at 298 K. P-loop (red), switch-I (orange) and switch-II (blue) are colored.

Res.	K-Ras-G12V-GTP				K-Ras-G12V-GDP			
	R_1 / s^{-1}	R_2 / s^{-1}	R_2 / R_1	^{15}N-{^1H} NOE	R_1 / s^{-1}	R_2 / s^{-1}	R_2 / R_1	^{15}N-{^1H} NOE
M1	1.04 ± 0.04	6.8 ± 0.2	6.5 ± 0.3	0.05	0.92 ± 0.02	8.1 ± 0.6	8.8 ± 0.6	0.44
T2	1.02 ± 0.03	11.2 ± 0.3	11.0 ± 0.4	0.48	1.05 ± 0.01	10.3 ± 0.3	9.8 ± 0.3	0.52
E3	0.81 ± 0.01	17.6 ± 1.0	21.6 ± 1.2	0.72	0.93 ± 0.01	16.4 ± 0.3	17.6 ± 0.4	0.76
Y4	0.76 ± 0.02	14.0 ± 0.6	18.3 ± 0.9	0.56	0.88 ± 0.01	14.0 ± 0.2	15.8 ± 0.2	0.80
K5	overlapping peaks				0.85 ± 0.01	14.9 ± 0.1	17.6 ± 0.2	0.81
L6	0.81 ± 0.02	17.3 ± 1.3	21.5 ± 1.7	0.85	0.90 ± 0.01	17.2 ± 0.3	19.2 ± 0.4	0.83
V7	0.89 ± 0.12	16.3 ± 0.8	18.3 ± 2.6	0.73	overlapping peaks			
V8	N/A	N/A	N/A	N/A	0.907 ± 0.003	18.9 ± 0.2	20.9 ± 0.2	0.83
V9	0.78 ± 0.01	18.7 ± 1.2	23.8 ± 1.6	0.86	0.89 ± 0.01	15.1 ± 0.4	17.0 ± 0.5	0.82
G10	0.79 ± 0.07	24.8 ± 5.9	31.3 ± 8.0	0.84	0.91 ± 0.01	17.5 ± 0.8	19.3 ± 0.9	0.83
A11	N/A	N/A	N/A	N/A	0.86 ± 0.01	14.4 ± 0.1	16.8 ± 0.2	0.86
V12	0.76 ± 0.03	19.1 ± 0.5	25.3 ± 1.3	0.81	overlapping peaks			
G13	0.82 ± 0.05	16.0 ± 1.5	19.6 ± 2.2	0.66	0.86 ± 0.01	16.8 ± 0.2	19.5 ± 0.4	0.84
V14	0.83 ± 0.02	18.4 ± 1.2	22.2 ± 1.6	0.83	0.94 ± 0.02	15.6 ± 0.2	16.5 ± 0.4	0.91
G15	0.88 ± 0.03	17.9 ± 2.1	20.3 ± 2.5	0.81	0.95 ± 0.02	18.2 ± 0.1	19.2 ± 0.5	0.90
K16	0.79 ± 0.07	18.2 ± 6.6	22.9 ± 8.6	0.77	0.87 ± 0.02	17.0 ± 0.5	19.5 ± 0.6	0.89
S17	0.87 ± 0.07	19.2 ± 3.9	22.1 ± 4.7	0.81	0.87 ± 0.01	16.5 ± 0.1	19.0 ± 0.3	0.87
A18	0.71 ± 0.03	17.8 ± 1.1	25.0 ± 1.9	0.68	0.87 ± 0.03	17.4 ± 0.4	19.9 ± 0.9	0.82
L19	0.81 ± 0.03	19.9 ± 0.7	24.4 ± 1.2	0.82	0.90 ± 0.01	15.7 ± 0.1	17.5 ± 0.2	0.91
T20	0.81 ± 0.04	22.3 ± 2.7	27.4 ± 3.6	0.77	0.91 ± 0.02	15.7 ± 0.4	17.2 ± 0.6	0.86
I21	0.76 ± 0.11	22.4 ± 3.5	29.7 ± 6.2	0.72	0.89 ± 0.03	16.9 ± 0.1	18.9 ± 0.5	0.82
Q22	N/A	N/A	N/A	N/A	0.91 ± 0.03	16.5 ± 0.3	18 ± 0.7	0.80
L23	0.76 ± 0.07	18.3 ± 1.3	24.2 ± 3.0	0.86	0.91 ± 0.02	16.3 ± 0.2	17.9 ± 0.5	0.86
I24	0.72 ± 0.03	21.4 ± 1.7	29.9 ± 2.6	0.71	0.88 ± 0.03	16.1 ± 0.2	18.3 ± 0.7	0.81
Q25	0.67 ± 0.05	21.0 ± 1.7	31.5 ± 3.4	0.89	0.87 ± 0.01	16.2 ± 0.1	18.7 ± 0.4	0.80
N26	0.79 ± 0.03	19.2 ± 0.8	24.4 ± 1.3	0.78	0.88 ± 0.01	15.5 ± 0.2	17.6 ± 0.4	0.87
H27	0.79 ± 0.03	17.1 ± 1.2	21.8 ± 1.7	0.69	0.92 ± 0.01	not fitted T_2 curve		0.78
F28	overlapping peaks				0.90 ± 0.03	14.3 ± 0.2	15.8 ± 0.6	0.84
V29	0.84 ± 0.17	11.3 ± 4.1	13.5 ± 5.7	0.68	0.89 ± 0.04	18.9 ± 0.5	21.3 ± 1.1	0.82
D30	N/A	N/A	N/A	N/A	1.09 ± 0.02	14.6 ± 0.3	13.4 ± 0.3	0.75
E31	N/A	N/A	N/A	N/A	overlapping peaks			
Y32	0.81 ± 0.05	23.4 ± 3.8	28.9 ± 5.0	0.91	0.99 ± 0.03	16.5 ± 0.3	16.7 ± 0.5	0.38
D33	N/A	N/A	N/A	N/A	0.85 ± 0.03	18.5 ± 0.2	21.8 ± 0.8	0.76
P34	N/A	N/A	N/A	N/A	N/A	N/A	N/A	N/A
T35	low intensity peak (not fitted)				0.92 ± 0.03	18.6 ± 0.3	20.2 ± 0.7	0.80
I36	N/A	N/A	N/A	N/A	0.90 ± 0.03	16.9 ± 0.1	18.7 ± 0.6	0.82
E37	N/A	N/A	N/A	N/A	0.94 ± 0.01	23.4 ± 1.7	24.7 ± 1.8	0.79
D38	N/A	N/A	N/A	N/A	0.89 ± 0.02	17.1 ± 0.2	19.1 ± 0.5	0.75
S39	0.73 ± 0.04	16.4 ± 1.5	22.3 ± 2.4	0.76	0.88 ± 0.02	14.9 ± 0.3	17.0 ± 0.4	0.76
Y40	overlapping peaks				0.86 ± 0.01	14.9 ± 0.3	17.4 ± 0.4	0.82
R41	overlapping peaks				0.89 ± 0.01	14.5 ± 0.1	16.2 ± 0.2	0.74
K42	0.79 ± 0.01	14.7 ± 0.5	18.7 ± 0.7	0.71	0.88 ± 0.01	14.4 ± 0.2	16.4 ± 0.3	0.76

Q43	0.81 ± 0.03	19.4 ± 0.3	24 ± 1.1	0.76	0.92 ± 0.01	17.4 ± 0.2	18.9 ± 0.4	0.76
V44	overlapping peaks				0.91 ± 0.01	14.8 ± 0.2	16.2 ± 0.2	0.81
V45	0.83 ± 0.05	14.4 ± 0.2	17.4 ± 1.1	0.77	0.889 ± 0.004	12.7 ± 0.2	14.3 ± 0.3	0.76
I46	0.72 ± 0.05	17.0 ± 0.8	23.6 ± 1.9	0.67	0.82 ± 0.01	16.6 ± 0.5	20.2 ± 0.6	0.80
D47	0.76 ± 0.04	18.7 ± 4.1	24.6 ± 5.6	0.83	0.90 ± 0.05	16.5 ± 0.7	18.4 ± 1.3	0.79
G48	0.77 ± 0.05	17.4 ± 0.4	22.6 ± 1.4	0.80	0.88 ± 0.04	14.9 ± 0.4	16.9 ± 1.0	0.80
E49	0.76 ± 0.01	16.9 ± 0.2	22.2 ± 0.5	0.82	0.89 ± 0.01	15.3 ± 0.1	17.3 ± 0.3	0.78
T50	0.78 ± 0.02	17.0 ± 0.7	21.7 ± 1.1	0.75	0.89 ± 0.03	16.1 ± 0.2	18 ± 0.6	0.76
C51	0.81 ± 0.05	17.0 ± 0.6	21.0 ± 1.5	0.82	0.96 ± 0.01	15.5 ± 0.2	16.1 ± 0.3	0.78
L52	0.79 ± 0.03	16.7 ± 0.9	21.0 ± 1.4	0.89	0.90 ± 0.01	14.3 ± 0.2	15.8 ± 0.3	0.78
L53	overlapping peaks				0.89 ± 0.01	14.0 ± 0.2	15.7 ± 0.3	0.83
D54	N/A	N/A	N/A	N/A	0.89 ± 0.01	16.3 ± 0.2	18.3 ± 0.3	0.80
I55	N/A	N/A	N/A	N/A	0.86 ± 0.01	14.2 ± 0.3	16.6 ± 0.3	0.83
L56	N/A	N/A	N/A	N/A	0.89 ± 0.02	18.9 ± 0.2	21.3 ± 0.5	0.82
D57	N/A	N/A	N/A	N/A	0.89 ± 0.01	19.5 ± 0.4	21.9 ± 0.5	0.83
T58	N/A	N/A	N/A	N/A	0.83 ± 0.01	19.0 ± 0.6	23.0 ± 0.8	0.82
A59	N/A	N/A	N/A	N/A	0.86 ± 0.02	15.7 ± 0.6	18.3 ± 0.8	0.73
G60	N/A	N/A	N/A	N/A	1.13 ± 0.03	12.3 ± 0.4	10.9 ± 0.4	0.62
Q61	N/A	N/A	N/A	N/A	overlapping peaks			
E62	N/A	N/A	N/A	N/A	1.07 ± 0.03	12.9 ± 0.7	12 ± 0.7	0.57
E63	N/A	N/A	N/A	N/A	overlapping peaks			
Y64	N/A	N/A	N/A	N/A	1.01 ± 0.01	16.3 ± 0.4	16.1 ± 0.5	0.60
S65	N/A	N/A	N/A	N/A	overlapping peaks			
A66	N/A	N/A	N/A	N/A	0.98 ± 0.04	20.1 ± 0.2	20.5 ± 0.8	0.78
M67	N/A	N/A	N/A	N/A	0.96 ± 0.04	15.4 ± 0.5	16.0 ± 0.8	0.72
R68	N/A	N/A	N/A	N/A	0.97 ± 0.02	15.6 ± 0.5	16.0 ± 0.6	0.85
D69	N/A	N/A	N/A	N/A	0.96 ± 0.01	16.4 ± 0.2	17.1 ± 0.3	0.78
Q70	N/A	N/A	N/A	N/A	0.90 ± 0.02	16.4 ± 0.1	18.2 ± 0.4	0.78
Y71	N/A	N/A	N/A	N/A	overlapping peaks			
M72	N/A	N/A	N/A	N/A	overlapping peaks			
R73	N/A	N/A	N/A	N/A	0.88 ± 0.02	17.2 ± 0.4	19.5 ± 0.6	0.76
T74	0.82 ± 0.11	18.4 ± 2.4	22.4 ± 4.3	0.67	0.93 ± 0.01	18.6 ± 0.3	20.0 ± 0.4	0.80
G75	0.87 ± 0.01	21.3 ± 0.4	24.6 ± 0.6	0.71	0.92 ± 0.01	19.0 ± 0.8	20.7 ± 0.9	0.84
E76	overlapping peaks				0.90 ± 0.02	14.5 ± 0.1	16.2 ± 0.4	0.80
G77	0.74 ± 0.01	16.4 ± 2.0	22.1 ± 2.7	0.77	0.85 ± 0.01	13.3 ± 0.4	15.7 ± 0.5	0.80
F78	0.81 ± 0.03	19.9 ± 2.1	24.6 ± 2.7	0.84	0.88 ± 0.02	15.1 ± 0.2	17.2 ± 0.4	0.83
L79	0.88 ± 0.07	21.0 ± 4.1	23.9 ± 5.0	0.86	0.90 ± 0.01	16.9 ± 0.3	18.6 ± 0.4	0.86
C80	0.68 ± 0.01	17.4 ± 0.5	25.7 ± 0.9	0.79	0.83 ± 0.01	15.6 ± 0.2	18.7 ± 0.3	0.79
V81	0.76 ± 0.04	20.9 ± 2.5	27.4 ± 3.5	0.77	0.87 ± 0.01	16.6 ± 0.1	19.0 ± 0.3	0.81
F82	0.81 ± 0.01	16.2 ± 0.7	20.0 ± 0.9	0.81	0.92 ± 0.01	15.1 ± 0.3	16.5 ± 0.4	0.84
A83	overlapping peaks				0.90 ± 0.02	15.1 ± 0.3	16.8 ± 0.5	0.83
I84	0.77 ± 0.01	15.8 ± 0.4	20.5 ± 0.5	0.79	0.86 ± 0.02	15.7 ± 0.3	18.3 ± 0.5	0.83
N85	overlapping peaks				0.93 ± 0.01	17.7 ± 0.2	19.1 ± 0.3	0.83
N86	0.8 ± 0.02	13.9 ± 0.4	17.3 ± 0.7	0.83	0.89 ± 0.03	16.7 ± 0.3	18.7 ± 0.7	0.80
T87	N/A	N/A	N/A	N/A	N/A	N/A	N/A	N/A
K88	0.84 ± 0.02	17.0 ± 0.7	20.3 ± 1.0	0.79	0.94 ± 0.01	15.1 ± 0.3	16.1 ± 0.4	0.82

S89	0.75 ± 0.02	17.9 ± 0.8	24.0 ± 1.2	0.80	0.86 ± 0.01	16.0 ± 0.4	18.7 ± 0.5	0.85
F90	0.80 ± 0.02	22.4 ± 0.9	28.1 ± 1.2	0.70	0.89 ± 0.01	17.8 ± 0.1	19.9 ± 0.3	0.87
E91	0.76 ± 0.02	18.1 ± 0.6	23.8 ± 1.1	0.75	0.88 ± 0.03	14.9 ± 0.1	16.9 ± 0.6	0.85
D92	0.78 ± 0.04	19.9 ± 1.5	25.6 ± 2.4	0.86	0.89 ± 0.01	16.2 ± 0.3	18.1 ± 0.5	0.87
I93	0.76 ± 0.04	17.9 ± 2.2	23.5 ± 3.2	0.82	0.9 ± 0.01	17.4 ± 0.5	19.3 ± 0.6	0.93
H94	0.81 ± 0.04	19.4 ± 1.7	23.9 ± 2.4	0.78	0.89 ± 0.01	17.2 ± 0.5	19.2 ± 0.6	0.90
H95	0.81 ± 0.05	21.5 ± 0.9	26.5 ± 2.0	0.74	0.91 ± 0.01	15.9 ± 0.2	17.5 ± 0.4	0.87
Y96	0.76 ± 0.06	19.6 ± 0.7	25.7 ± 2.1	0.75	0.86 ± 0.02	16.3 ± 0.2	19.0 ± 0.6	0.70
R97	overlapping peaks				0.87 ± 0.01	16.4 ± 0.3	18.8 ± 0.4	0.79
E98	0.83 ± 0.02	19.9 ± 0.6	24 ± 0.9	0.81	overlapping peaks			
Q99	overlapping peaks				overlapping peaks			
I100	0.79 ± 0.06	18.4 ± 0.4	23.3 ± 1.9	0.74	0.89 ± 0.02	16.4 ± 0.2	18.4 ± 0.5	0.84
K101	overlapping peaks				0.90 ± 0.02	16.4 ± 0.1	18.2 ± 0.3	0.78
R102	0.78 ± 0.03	17.9 ± 0.5	23 ± 1.2	0.82	0.91 ± 0.01	17.1 ± 0.2	18.8 ± 0.2	0.77
V103	N/A	N/A	N/A	N/A	overlapping peaks			
K104	0.82 ± 0.04	17.7 ± 0.9	21.6 ± 1.5	0.74	0.91 ± 0.02	16.31 ± 0.04	17.9 ± 0.4	0.79
D105	0.81 ± 0.02	17.6 ± 0.3	21.6 ± 0.8	0.74	0.92 ± 0.02	15.1 ± 0.3	16.4 ± 0.5	0.73
S106	0.79 ± 0.01	17.3 ± 0.4	22.0 ± 0.6	0.64	0.92 ± 0.01	15.6 ± 0.1	17.0 ± 0.2	0.71
E107	0.83 ± 0.02	13.7 ± 0.9	16.5 ± 1.1	0.62	overlapping peaks			
D108	0.86 ± 0.03	14.9 ± 0.4	17.4 ± 0.8	0.55	overlapping peaks			
V109	0.87 ± 0.03	11.6 ± 0.5	13.4 ± 0.8	0.28	0.93 ± 0.01	9.7 ± 0.1	10.4 ± 0.2	0.39
P110	N/A	N/A	N/A	N/A	N/A	N/A	N/A	N/A
M111	0.82 ± 0.01	14.9 ± 0.2	18.2 ± 0.3	0.86	0.89 ± 0.02	13.5 ± 0.3	15.2 ± 0.5	0.66
V112	0.79 ± 0.03	17.1 ± 0.5	21.5 ± 1.0	0.81	overlapping peaks			
L113	0.81 ± 0.03	22.2 ± 0.3	27.3 ± 1.0	0.77	0.91 ± 0.01	17.6 ± 0.2	19.3 ± 0.3	0.84
V114	0.78 ± 0.05	20.1 ± 1.8	25.7 ± 2.8	0.84	0.94 ± 0.01	17.7 ± 0.2	18.9 ± 0.3	0.87
G115	0.77 ± 0.02	19.3 ± 0.5	24.9 ± 0.9	0.80	0.86 ± 0.01	14.0 ± 0.3	16.2 ± 0.4	0.87
N116	0.79 ± 0.02	16.5 ± 0.7	20.9 ± 1.0	0.89	0.88 ± 0.01	15.2 ± 0.4	17.3 ± 0.5	0.81
K117	0.69 ± 0.03	19.7 ± 2.8	28.4 ± 4.2	0.82	0.86 ± 0.01	18.4 ± 1.3	21.3 ± 1.6	0.90
C118	0.79 ± 0.03	19.2 ± 1.4	24.2 ± 2.1	0.86	0.84 ± 0.02	16.9 ± 0.1	20.1 ± 0.5	0.87
D119	0.78 ± 0.02	19.5 ± 0.9	25.2 ± 1.4	0.84	0.93 ± 0.02	17.7 ± 0.4	18.9 ± 0.5	0.86
L120	0.77 ± 0.02	19.9 ± 0.2	26.0 ± 0.8	0.80	0.91 ± 0.03	16.9 ± 0.2	18.5 ± 0.7	0.80
P121	N/A	N/A	N/A	N/A	N/A	N/A	N/A	N/A
S122	0.78 ± 0.07	15.0 ± 0.3	19.4 ± 1.7	0.63	0.85 ± 0.03	12.8 ± 0.3	15 ± 0.6	0.65
R123	overlapping peaks				overlapping peaks			
T124	0.72 ± 0.07	14.6 ± 1.2	20.3 ± 2.6	0.69	0.90 ± 0.02	15.4 ± 0.2	17.2 ± 0.5	0.80
V125	0.76 ± 0.02	20.4 ± 1.4	26.7 ± 2.0	0.82	0.85 ± 0.02	15.1 ± 1.6	17.7 ± 1.9	0.84
D126	0.86 ± 0.01	18.7 ± 0.4	21.8 ± 0.6	0.73	0.96 ± 0.02	16.3 ± 0.2	17.1 ± 0.4	0.76
T127	overlapping peaks				0.92 ± 0.01	16.5 ± 0.7	17.9 ± 0.8	0.82
K128	0.85 ± 0.02	18.2 ± 0.5	21.5 ± 0.8	0.69	overlapping peaks			
Q129	0.80 ± 0.01	17.6 ± 0.2	21.9 ± 0.4	0.66	0.90 ± 0.01	15.1 ± 0.1	16.7 ± 0.2	0.69
A130	0.82 ± 0.01	16.8 ± 0.5	20.4 ± 0.6	0.80	0.91 ± 0.01	15.2 ± 0.2	16.8 ± 0.3	0.84
Q131	overlapping peaks				0.89 ± 0.01	17.0 ± 0.2	19.1 ± 0.3	0.85
D132	0.77 ± 0.02	19.2 ± 0.4	24.8 ± 0.8	0.77	0.87 ± 0.02	16.0 ± 0.2	18.3 ± 0.4	0.80
L133	0.77 ± 0.03	17.7 ± 0.7	22.9 ± 1.2	0.75	0.90 ± 0.01	15.3 ± 0.1	16.9 ± 0.2	0.83
A134	0.80 ± 0.01	17.1 ± 0.4	21.5 ± 0.6	0.89	0.91 ± 0.01	16.6 ± 0.3	18.2 ± 0.4	0.84

R135	0.77 ± 0.02	20.4 ± 0.3	26.5 ± 0.8	0.84	0.88 ± 0.01	17.1 ± 0.3	19.4 ± 0.4	0.90
S136	0.75 ± 0.01	19.8 ± 0.4	26.3 ± 0.6	0.85	overlapping peaks			
Y137	overlapping peaks				0.87 ± 0.02	14.8 ± 0.5	17.0 ± 0.7	0.81
G138	0.72 ± 0.01	18.1 ± 0.9	25.0 ± 1.3	0.87	0.86 ± 0.01	15.1 ± 0.1	17.5 ± 0.2	0.84
I139	0.77 ± 0.02	17.9 ± 0.7	23.4 ± 1.1	0.85	0.88 ± 0.01	16.7 ± 0.4	18.9 ± 0.6	0.87
P140	N/A	N/A	N/A	N/A	N/A	N/A	N/A	N/A
F141	0.70 ± 0.02	15.2 ± 0.3	21.6 ± 0.6	0.81	overlapping peaks			
I142	0.86 ± 0.01	17.9 ± 0.5	20.9 ± 0.7	0.84	0.918 ± 0.004	16.2 ± 0.2	17.7 ± 0.3	0.82
E143	0.76 ± 0.01	16.6 ± 0.7	22.0 ± 0.9	0.71	0.87 ± 0.02	15.0 ± 0.4	17.2 ± 0.5	0.76
T144	0.79 ± 0.02	17.3 ± 0.7	21.8 ± 1.1	0.87	0.86 ± 0.02	15.2 ± 0.2	17.6 ± 0.4	0.81
S145	0.72 ± 0.01	16.1 ± 1.3	22.3 ± 1.8	0.89	0.851 ± 0.003	15.3 ± 0.1	18.0 ± 0.1	0.85
A146	0.76 ± 0.02	23.5 ± 1.4	30.7 ± 2.0	0.87	0.89 ± 0.01	18.1 ± 0.3	20.4 ± 0.4	0.88
K147	0.76 ± 0.02	19.0 ± 1.2	25.2 ± 1.8	0.8	0.86 ± 0.01	15.9 ± 0.1	18.5 ± 0.4	0.83
T148	0.80 ± 0.03	19.7 ± 1.5	24.6 ± 2.1	0.74	0.88 ± 0.01	15.2 ± 0.3	17.3 ± 0.4	0.86
R149	0.84 ± 0.02	19.7 ± 1.3	23.4 ± 1.6	0.75	overlapping peaks			
Q150	0.73 ± 0.03	18.3 ± 1.2	25.1 ± 2.0	0.73	0.78 ± 0.01	14.2 ± 0.7	18.3 ± 0.9	0.71
G151	0.86 ± 0.02	17.9 ± 0.6	20.8 ± 0.8	0.8	0.93 ± 0.02	15.4 ± 0.5	16.5 ± 0.6	0.81
V152	0.78 ± 0.02	18.3 ± 0.5	23.5 ± 0.9	0.79	0.93 ± 0.01	16.0 ± 0.2	17.2 ± 0.3	0.84
D153	overlapping peaks				0.87 ± 0.01	16.0 ± 0.2	18.3 ± 0.3	0.88
D154	0.76 ± 0.02	18.5 ± 0.4	24.4 ± 0.8	0.82	0.86 ± 0.01	16.0 ± 0.2	18.6 ± 0.3	0.86
A155	0.82 ± 0.02	18.4 ± 0.8	22.5 ± 1.2	0.84	0.92 ± 0.01	15.8 ± 0.2	17.2 ± 0.3	0.86
F156	0.79 ± 0.01	16.3 ± 0.6	20.7 ± 0.8	0.79	0.88 ± 0.01	14.7 ± 0.5	16.6 ± 0.6	0.88
Y157	0.76 ± 0.01	20.4 ± 0.4	26.9 ± 0.6	0.78	0.88 ± 0.02	16.7 ± 0.3	19.0 ± 0.5	0.83
T158	0.79 ± 0.02	19.3 ± 0.7	24.4 ± 1.1	0.88	0.86 ± 0.01	17.1 ± 0.2	19.8 ± 0.4	0.81
L159	0.8 ± 0.02	17.6 ± 0.3	21.9 ± 0.7	0.80	0.92 ± 0.01	16.1 ± 0.4	17.5 ± 0.4	0.83
V160	overlapping peaks				overlapping peaks			
R161	0.78 ± 0.02	18.2 ± 0.4	23.4 ± 0.8	0.81	0.88 ± 0.02	16.6 ± 0.2	18.8 ± 0.4	0.82
E162	0.82 ± 0.03	20.4 ± 0.9	25.1 ± 1.4	0.79	0.89 ± 0.01	16.1 ± 0.2	18.2 ± 0.3	0.81
I163	overlapping peaks				0.89 ± 0.01	14.9 ± 0.1	16.7 ± 0.2	0.86
R164	0.81 ± 0.03	17.2 ± 0.6	21.3 ± 1.1	0.77	0.96 ± 0.03	14.0 ± 0.2	14.7 ± 0.6	0.73
K165	overlapping peaks				0.90 ± 0.01	15.9 ± 0.1	17.6 ± 0.2	0.86
H166	0.82 ± 0.02	17.7 ± 0.4	21.6 ± 0.7	0.74	0.99 ± 0.03	14.9 ± 0.1	15.1 ± 0.4	0.74
K167	0.90 ± 0.02	14.1 ± 0.2	15.6 ± 0.4	0.60	1.01 ± 0.01	13.7 ± 0.2	13.5 ± 0.2	0.62
E168	1.05 ± 0.03	12.3 ± 0.3	11.7 ± 0.5	0.49	overlapping peaks			
K169	1.25 ± 0.01	5.6 ± 0.3	4.5 ± 0.2	0.14	1.25 ± 0.01	5.0 ± 0.1	4.0 ± 0.1	0.13

Table S3 Extended model-free parameters (S^2, S^2_s, S^2_f, τ_e, R_{ex}) of K-Ras-G12V·Mg^{2+} bound to GTP and GDP recorded at 700 MHz at 298 K. P-loop (red), switch-I (orange) and switch-II (blue) are colored.

Res.	K-Ras-G12V-GTP				
	S^2	S^2_s	S^2_f	τ_e / ps	R_{ex} / s^{-1}
M1	N/A	N/A	N/A	N/A	N/A
T2	0.52 ± 0.02	0.78 ± 0.02	0.66 ± 0.02	1010 ± 91	-
E3	0.89 ± 0.01	1	0.89 ± 0.01	-	-
Y4	0.67 ± 0.03	0.77 ± 0.02	0.88 ± 0.02	579 ± 132	-
K5			overlapping peaks		
L6	0.88 ± 0.02	1	0.88 ± 0.02	-	-
V7	0.81 ± 0.04	1	0.81 ± 0.04	20 ± 10	-
V8	N/A	N/A	N/A	N/A	N/A
V9	0.86 ± 0.01	1	0.86 ± 0.01	-	-
G10	0.90 ± 0.08	1	0.90 ± 0.08	-	-
A11	N/A	N/A	N/A	N/A	N/A
V12	0.9 ± 0.02	1	0.9 ± 0.02	-	-
G13	0.83 ± 0.04	1	0.83 ± 0.04	37 ± 15	-
V14	0.91 ± 0.02	1	0.91 ± 0.02	-	-
G15	0.96 ± 0.03	1	0.96 ± 0.03	-	-
K16	0.87 ± 0.07	1	0.87 ± 0.07	-	-
S17	0.96 ± 0.07	1	0.96 ± 0.07	-	-
A18	0.81 ± 0.03	1	0.81 ± 0.03	-	-
L19	0.92 ± 0.02	1	0.92 ± 0.02	-	-
T20	0.92 ± 0.04	1	0.92 ± 0.04	-	-
I21	0.91 ± 0.1	1	0.91 ± 0.1	-	-
Q22	N/A	N/A	N/A	N/A	N/A
L23	0.87 ± 0.05	1	0.87 ± 0.05	-	-
I24	0.82 ± 0.03	1	0.82 ± 0.03	-	-
Q25	0.73 ± 0.05	1	0.73 ± 0.05	-	6 ± 2
N26	0.89 ± 0.02	1	0.89 ± 0.02	-	-
H27	0.83 ± 0.03	1	0.83 ± 0.03	30 ± 10	-
F28			overlapping peaks		
V29	0.74 ± 0.14	1	0.74 ± 0.14	19 ± 14	-
D30	N/A	N/A	N/A	N/A	N/A
E31	N/A	N/A	N/A	N/A	N/A
Y32	0.91 ± 0.06	1	0.91 ± 0.06	-	-
D33	N/A	N/A	N/A	N/A	N/A
P34	N/A	N/A	N/A	N/A	N/A
T35	N/A	N/A	N/A	N/A	N/A
I36	N/A	N/A	N/A	N/A	N/A
E37	N/A	N/A	N/A	N/A	N/A
D38	N/A	N/A	N/A	N/A	N/A
S39	0.80 ± 0.04	1	0.80 ± 0.04	-	-
Y40			overlapping peaks		
R41			overlapping peaks		
K42	0.71 ± 0.02	0.78 ± 0.02	0.91 ± 0.02	907 ± 237	-

Q43	0.94 ± 0.02	1	0.94 ± 0.02	-	-
V44			overlapping peaks		
V45	0.71 ± 0.01	1	0.71 ± 0.01	-	-
I46	0.80 ± 0.03	1	0.80 ± 0.03	28 ± 9	-
D47	0.84 ± 0.05	1	0.84 ± 0.05	-	-
G48	0.85 ± 0.02	1	0.85 ± 0.02	-	-
E49	0.83 ± 0.01	1	0.83 ± 0.01	-	-
T50	0.85 ± 0.02	1	0.85 ± 0.02	-	-
C51	0.85 ± 0.03	1	0.85 ± 0.03	-	-
L52	0.85 ± 0.03	1	0.85 ± 0.03	-	-
L53			overlapping peaks		
D54	N/A	N/A	N/A	N/A	N/A
I55	N/A	N/A	N/A	N/A	N/A
L56	N/A	N/A	N/A	N/A	N/A
D57	N/A	N/A	N/A	N/A	N/A
T58	N/A	N/A	N/A	N/A	N/A
A59	N/A	N/A	N/A	N/A	N/A
G60	N/A	N/A	N/A	N/A	N/A
Q61	N/A	N/A	N/A	N/A	N/A
E62	N/A	N/A	N/A	N/A	N/A
E63	N/A	N/A	N/A	N/A	N/A
Y64	N/A	N/A	N/A	N/A	N/A
S65	N/A	N/A	N/A	N/A	N/A
A66	N/A	N/A	N/A	N/A	N/A
M67	N/A	N/A	N/A	N/A	N/A
R68	N/A	N/A	N/A	N/A	N/A
D69	N/A	N/A	N/A	N/A	N/A
Q70	N/A	N/A	N/A	N/A	N/A
Y71	N/A	N/A	N/A	N/A	N/A
M72	N/A	N/A	N/A	N/A	N/A
R73	N/A	N/A	N/A	N/A	N/A
T74	0.88 ± 0.08	1	0.88 ± 0.08	52 ± 46	-
G75	0.92 ± 0.02	1	0.92 ± 0.02	67 ± 21	2.5 ± 0.5
E76			overlapping peaks		
G77	0.82 ± 0.01	1	0.82 ± 0.01	-	-
F78	0.9 ± 0.04	1	0.9 ± 0.04	-	-
L79	0.98 ± 0.07	1	0.98 ± 0.07	-	-
C80	0.75 ± 0.02	1	0.75 ± 0.02	-	2.2 ± 0.6
V81	0.86 ± 0.04	1	0.86 ± 0.04	-	-
F82	0.89 ± 0.01	1	0.89 ± 0.01	-	-
A83			overlapping peaks		
I84	0.83 ± 0.01	1	0.83 ± 0.01	0 ± 0	0 ± 0
N85			overlapping peaks		
N86	N/A	N/A	N/A	N/A	N/A
T87	N/A	N/A	N/A	N/A	N/A
K88	0.89 ± 0.02	1	0.89 ± 0.02	-	-

S89	0.83 ± 0.02	1	0.83 ± 0.02	-	-
F90	0.85 ± 0.02	1	0.85 ± 0.02	31 ± 10	5.1 ± 1
E91	0.86 ± 0.02	1	0.86 ± 0.02	-	-
D92	0.89 ± 0.04	1	0.89 ± 0.04	-	-
I93	0.84 ± 0.04	1	0.84 ± 0.04	-	-
H94	0.90 ± 0.04	1	0.90 ± 0.04	-	-
H95	0.99 ± 0.04	1	0.99 ± 0.04	-	-
Y96	0.93 ± 0.03	1	0.93 ± 0.03	-	-
R97			overlapping peaks		
E98	0.94 ± 0.02	1	0.94 ± 0.02	-	-
Q99			overlapping peaks		
I100	0.90 ± 0.02	1	0.90 ± 0.02	-	-
K101			overlapping peaks		
R102	0.87 ± 0.02	1	0.87 ± 0.02	-	-
V103	N/A	N/A	N/A	N/A	N/A
K104	0.89 ± 0.03	1	0.89 ± 0.03	-	-
D105	0.86 ± 0.01	1	0.86 ± 0.01	29 ± 12	-
S106	0.83 ± 0.01	1	0.83 ± 0.01	38 ± 8	-
E107	0.66 ± 0.04	0.78 ± 0.03	0.847 ± 0.027	900 ± 168	-
D108	0.72 ± 0.03	0.84 ± 0.02	0.855 ± 0.02	663 ± 114	-
V109	0.55 ± 0.03	0.77 ± 0.03	0.708 ± 0.026	642 ± 61	-
P110	N/A	N/A	N/A	N/A	N/A
M111	N/A	N/A	N/A	N/A	N/A
V112	0.85 ± 0.02	1	0.85 ± 0.02	-	-
L113	0.88 ± 0.03	1	0.88 ± 0.03	21 ± 13	4.3 ± 0.7
V114	0.89 ± 0.04	1	0.89 ± 0.04	-	-
G115	0.85 ± 0.02	1	0.85 ± 0.02	-	1.9 ± 0.7
N116	0.85 ± 0.02	1	0.85 ± 0.02	-	-
K117	0.77 ± 0.03	1	0.77 ± 0.03	-	-
C118	0.88 ± 0.03	1	0.88 ± 0.03	-	-
D119	0.88 ± 0.02	1	0.88 ± 0.02	-	-
L120	0.84 ± 0.03	1	0.84 ± 0.03	-	2.7 ± 0.5
P121	N/A	N/A	N/A	N/A	N/A
S122	0.74 ± 0.01	1	0.74 ± 0.01	25 ± 6	-
R123			overlapping peaks		
T124	0.73 ± 0.05	1	0.73 ± 0.05	16 ± 6	-
V125	0.85 ± 0.02	1	0.85 ± 0.02	-	-
D126	0.92 ± 0.01	1	0.92 ± 0.01	50 ± 19	-
T127			overlapping peaks		
K128	0.89 ± 0.02	1	0.89 ± 0.02	54 ± 16	-
Q129	0.86 ± 0.01	1	0.86 ± 0.01	39 ± 10	-
A130	0.89 ± 0.01	1	0.89 ± 0.01	-	-
Q131			overlapping peaks		
D132	0.89 ± 0.02	1	0.89 ± 0.02	-	-
L133	0.86 ± 0.02	1	0.86 ± 0.02	-	-
A134	0.86 ± 0.01	1	0.86 ± 0.01	-	-

R135	0.85 ± 0.02	1	0.85 ± 0.02	-	3.1 ± 0.5
S136	0.83 ± 0.01	1	0.83 ± 0.01	-	2.9 ± 0.5
Y137			overlapping peaks		
G138	0.80 ± 0.01	1	0.80 ± 0.01	-	-
I139	0.85 ± 0.02	1	0.85 ± 0.02	-	-
P140	N/A	N/A	N/A	N/A	N/A
F141	0.76 ± 0.01	1	0.76 ± 0.01	-	-
I142	0.93 ± 0.01	1	0.93 ± 0.01	-	-
E143	0.8 ± 0.01	1	0.8 ± 0.01	22 ± 7	-
T144	0.87 ± 0.02	1	0.87 ± 0.02	-	-
S145	0.8 ± 0.02	1	0.8 ± 0.02	-	-
A146	0.84 ± 0.02	1	0.84 ± 0.02	-	6.3 ± 1.4
K147	0.85 ± 0.02	1	0.85 ± 0.02	-	-
T148	0.89 ± 0.03	1	0.89 ± 0.03	-	-
R149	0.93 ± 0.02	1	0.93 ± 0.02	-	-
Q150	0.83 ± 0.03	1	0.83 ± 0.03	-	-
G151	0.92 ± 0.02	1	0.92 ± 0.02	-	-
V152	0.87 ± 0.02	1	0.87 ± 0.02	-	-
D153			overlapping peaks		
D154	0.83 ± 0.02	1	0.83 ± 0.02	-	1.5 ± 0.6
A155	0.90 ± 0.02	1	0.90 ± 0.02	-	-
F156	0.85 ± 0.01	1	0.85 ± 0.01	-	-
Y157	0.83 ± 0.01	1	0.83 ± 0.01	-	3.4 ± 0.4
T158	0.89 ± 0.02	1	0.89 ± 0.02	-	-
L159	0.87 ± 0.01	1	0.87 ± 0.01	-	-
V160			overlapping peaks		
R161	0.88 ± 0.02	1	0.88 ± 0.02	-	-
E162	0.93 ± 0.03	1	0.93 ± 0.03	-	-
I163			overlapping peaks		
R164	0.86 ± 0.02	1	0.86 ± 0.02	-	-
K165			overlapping peaks		
H166	0.87 ± 0.02	1	0.87 ± 0.02	30 ± 12	-
K167	0.67 ± 0.02	0.82 ± 0.01	0.82 ± 0.01	941 ± 129	-
E168	0.57 ± 0.02	0.83 ± 0.02	0.69 ± 0.02	992 ± 94	-
K169	N/A	N/A	N/A	N/A	N/A

Res.	K-Ras-G12V-GDP				
	S^2	S^2_s	S^2_f	τ_e / ps	R_{ex} / s^{-1}
M1	N/A	N/A	N/A	N/A	N/A
T2	0.54 ± 0.02	0.78 ± 0.02	0.69 ± 0.02	999 ± 102	-
E3	0.90 ± 0.01	1	0.9 ± 0.01	-	-
Y4	N/A	N/A	N/A	N/A	N/A
K5	0.829 ± 003	1	0.829 ± 003	-	-
L6	0.86 ± 0.01	1	0.86 ± 0.01	-	1.7 ± 0.3
V7			overlapping peaks		
V8	0.875 ± 003	1	0.875 ± 003	-	3.2 ± 0.2
V9	0.85 ± 0.01	1	0.85 ± 0.01	-	-
G10	0.88 ± 0.01	1	0.88 ± 0.01	-	-
A11	0.820 ± 004	1	0.820 ± 004	-	-
V12			overlapping peaks		
G13	0.83 ± 0.01	1	0.83 ± 0.01	-	1.9 ± 0.3
V14	0.88 ± 0.01	1	0.88 ± 0.01	-	-
G15	0.91 ± 0.02	1	0.91 ± 0.02	-	1.8 ± 0.4
K16	0.84 ± 0.02	1	0.84 ± 0.02	-	2.0 ± 0.5
S17	0.84 ± 0.01	1	0.84 ± 0.01	-	1.5 ± 0.3
A18	0.84 ± 0.03	1	0.84 ± 0.03	-	2.3 ± 0.7
L19	0.871 ± 004	1	0.871 ± 004	-	-
T20	0.88 ± 0.02	1	0.88 ± 0.02	-	-
I21	0.86 ± 0.02	1	0.86 ± 0.02	-	1.5 ± 0.4
Q22	0.91 ± 0.01	1	0.91 ± 0.01	-	-
L23	0.9 ± 0.01	1	0.9 ± 0.01	-	-
I24	0.89 ± 0.01	1	0.89 ± 0.01	-	-
Q25	0.83 ± 0.01	1	0.83 ± 0.01	-	1.2 ± 0.3
N26	0.86 ± 0.01	1	0.86 ± 0.01	-	-
H27	N/A	N/A	N/A	N/A	N/A
F28	0.81 ± 0.01	1	0.81 ± 0.01	-	-
V29	0.86 ± 0.04	1	0.86 ± 0.04	-	3.6 ± 0.8
D30	N/A	N/A	N/A	N/A	N/A
E31			overlapping peaks		
Y32	0.84 ± 0.02	1	0.84 ± 0.02	158 ± 45	1.4 ± 0.5
D33	0.82 ± 0.03	1	0.82 ± 0.03	-	3.8 ± 0.6
P34	N/A	N/A	N/A	N/A	N/A
T35	0.89 ± 0.03	1	0.89 ± 0.03	-	2.7 ± 0.6
I36	0.87 ± 0.03	1	0.87 ± 0.03	-	1.3 ± 0.5
E37	0.91 ± 0.01	1	0.91 ± 0.01	-	7.0 ± 1.7
D38	0.84 ± 0.02	1	0.84 ± 0.02	23 ± 11	2.0 ± 0.4
S39	0.84 ± 0.01	1	0.84 ± 0.01	-	-
Y40	0.83 ± 0.01	1	0.83 ± 0.01	-	-
R41	N/A	N/A	N/A	N/A	N/A
K42	0.81 ± 0.01	1	0.81 ± 0.01	24 ± 8	-
Q43	0.89 ± 0.01	1	0.89 ± 0.01	-	1.5 ± 0.3
V44	N/A	N/A	N/A	N/A	N/A

V45	N/A	N/A	N/A	N/A	N/A
I46	0.80 ± 0.01	1	0.80 ± 0.01	-	2.4 ± 0.5
D47	0.90 ± 0.03	1	0.90 ± 0.03	-	-
G48	0.84 ± 0.02	1	0.84 ± 0.02	-	-
E49	0.85 ± 0.01	1	0.85 ± 0.01	-	-
T50	0.89 ± 0.01	1	0.89 ± 0.01	-	-
C51	0.90 ± 0.01	1	0.90 ± 0.01	-	-
L52	N/A	N/A	N/A	N/A	N/A
L53	N/A	N/A	N/A	N/A	N/A
D54	0.86 ± 0.01	1	0.86 ± 0.01	-	0.9 ± 0.3
I55	0.82 ± 0.01	1	0.82 ± 0.01	-	-
L56	0.86 ± 0.02	1	0.86 ± 0.02	-	3.5 ± 0.3
D57	0.86 ± 0.01	1	0.86 ± 0.01	-	4.1 ± 0.5
T58	0.80 ± 0.01	1	0.80 ± 0.01	-	4.7 ± 0.7
A59	0.84 ± 0.02	1	0.84 ± 0.02	-	-
G60	0.65 ± 0.02	0.86 ± 0.02	0.76 ± 0.02	1130 ± 161	0 ± 0
Q61			overlapping peaks		
E62	0.7 ± 0.03	0.88 ± 0.03	0.79 ± 0.03	890 ± 134	0 ± 0
E63			overlapping peaks		
Y64	0.91 ± 0.01	1	0.91 ± 0.01	154 ± 39	0 ± 0
S65			overlapping peaks		
A66	0.93 ± 0.04	1	0.93 ± 0.04	41 ± 32	3.4 ± 0.7
M67	0.88 ± 0.02	1	0.88 ± 0.02	45 ± 18	-
R68	0.92 ± 0.02	1	0.92 ± 0.02	-	-
D69	0.92 ± 0.01	1	0.92 ± 0.01	-	-
Q70	0.91 ± 0.01	1	0.91 ± 0.01	-	-
Y71			overlapping peaks		
M72			overlapping peaks		
R73	0.85 ± 0.02	1	0.85 ± 0.02	-	2.0 ± 0.5
T74	0.90 ± 0.01	1	0.90 ± 0.01	-	2.6 ± 0.4
G75	0.89 ± 0.01	1	0.89 ± 0.01	-	3.1 ± 0.8
E76	0.82 ± 0.01	1	0.82 ± 0.01	-	-
G77	0.82 ± 0.01	1	0.82 ± 0.01	-	-
F78	0.84 ± 0.01	1	0.84 ± 0.01	-	-
L79	0.87 ± 0.01	1	0.87 ± 0.01	-	1.2 ± 0.3
C80	0.81 ± 0.01	1	0.81 ± 0.01	-	1.2 ± 0.3
V81	0.84 ± 0.01	1	0.84 ± 0.01	-	1.5 ± 0.2
F82	0.88 ± 0.01	1	0.88 ± 0.01	-	-
A83	0.85 ± 0.01	1	0.85 ± 0.01	-	-
I84	0.85 ± 0.01	1	0.85 ± 0.01	-	-
N85	0.89 ± 0.01	1	0.89 ± 0.01	-	1.7 ± 0.3
N86	0.86 ± 0.03	1	0.86 ± 0.03	-	1.3 ± 0.6
T87	N/A	N/A	N/A	N/A	N/A
K88	0.88 ± 0.01	1	0.88 ± 0.01	-	-
S89	0.83 ± 0.01	1	0.83 ± 0.01	-	1.2 ± 0.4
F90	0.86 ± 0.01	1	0.86 ± 0.01	-	2.4 ± 0.2

E91	0.83 ± 0.01	1	0.83 ± 0.01	-	-
D92	0.87 ± 0.01	1	0.87 ± 0.01	-	-
I93	0.87 ± 0.01	1	0.87 ± 0.01	-	1.8 ± 0.6
H94	0.86 ± 0.01	1	0.86 ± 0.01	-	1.8 ± 0.5
H95	0.88 ± 0.01	1	0.88 ± 0.01	-	-
Y96	0.89 ± 0.01	1	0.89 ± 0.01	-	-
R97	0.84 ± 0.01	1	0.84 ± 0.01	-	1.3 ± 0.3
E98			overlapping peaks		
Q99			overlapping peaks		
I100	0.91 ± 0.01	1	0.91 ± 0.01	-	-
K101	0.914 ± 0.004	1	0.914 ± 0.004	-	-
R102	0.88 ± 0.01	1	0.88 ± 0.01	-	1.4 ± 0.2
V103			overlapping peaks		
K104	0.910 ± 0.002	1	0.910 ± 0.002	-	-
D105	0.85 ± 0.01	1	0.85 ± 0.01	34 ± 12	-
S106	0.87 ± 0.01	1	0.87 ± 0.01	30 ± 9	-
E107			overlapping peaks		
D108			overlapping peaks		
V109	0.52 ± 0.01	0.74 ± 0.01	0.7 ± 0.01	750 ± 60	-
P110	N/A	N/A	N/A	N/A	N/A
M111	0.75 ± 0.02	0.82 ± 0.02	0.91 ± 0.02	603 ± 164	-
V112			overlapping peaks		
L113	0.88 ± 0.01	1	0.88 ± 0.01	-	1.9 ± 0.2
V114	0.90 ± 0.01	1	0.90 ± 0.01	-	1.6 ± 0.2
G115	0.83 ± 0.01	1	0.83 ± 0.01	-	-
N116	0.85 ± 0.01	1	0.85 ± 0.01	-	-
K117	0.83 ± 0.01	1	0.83 ± 0.01	-	3.5 ± 1.3
C118	0.81 ± 0.02	1	0.81 ± 0.02	-	2.4 ± 0.4
D119	0.90 ± 0.02	1	0.90 ± 0.02	-	1.5 ± 0.5
L120	0.93 ± 0.01	1	0.93 ± 0.01	-	-
P121	N/A	N/A	N/A	N/A	N/A
S122	0.71 ± 0.02	0.78 ± 0.02	0.9 ± 0.02	611 ± 170	-
R123			overlapping peaks		
T124	0.86 ± 0.01	1	0.86 ± 0.01	-	-
V125	0.83 ± 0.02	1	0.83 ± 0.02	-	-
D126	0.92 ± 0.01	1	0.92 ± 0.01	-	-
T127	0.89 ± 0.01	1	0.89 ± 0.01	-	-
K128			overlapping peaks		
Q129	0.84 ± 0.01	1	0.84 ± 0.01	33 ± 7	-
A130	0.87 ± 0.01	1	0.87 ± 0.01	-	-
Q131	0.86 ± 0.01	1	0.86 ± 0.01	-	1.6 ± 0.2
D132	0.84 ± 0.02	1	0.84 ± 0.02	-	0.9 ± 0.3
L133	0.87 ± 0.01	1	0.87 ± 0.01	-	-
A134	0.89 ± 0.01	1	0.89 ± 0.01	-	-
R135	0.85 ± 0.01	1	0.85 ± 0.01	-	1.9 ± 0.3
S136			overlapping peaks		

Y137	0.84 ± 0.02	1	0.84 ± 0.02	-	-
G138	0.836 ± 0.004	1	0.836 ± 0.004	-	-
I139	0.85 ± 0.01	1	0.85 ± 0.01	-	1.4 ± 0.5
P140	N/A	N/A	N/A	N/A	N/A
F141			overlapping peaks		
I142	0.888 ± 0.004	1	0.888 ± 0.004	-	-
E143	0.84 ± 0.01	1	0.84 ± 0.01	-	-
T144	0.84 ± 0.01	1	0.84 ± 0.01	-	-
S145	0.821 ± 0.003	1	0.821 ± 0.003	-	0.6 ± 0.1
A146	0.86 ± 0.01	1	0.86 ± 0.01	-	2.7 ± 0.3
K147	0.83 ± 0.01	1	0.83 ± 0.01	-	1.0 ± 0.3
T148	0.85 ± 0.01	1	0.85 ± 0.01	-	-
R149			overlapping peaks		
Q150	0.75 ± 0.01	1	0.75 ± 0.01	-	-
G151	0.89 ± 0.01	1	0.89 ± 0.01	-	-
V152	0.90 ± 0.01	1	0.90 ± 0.01	-	-
D153	0.84 ± 0.01	1	0.84 ± 0.01	-	0.9 ± 0.3
D154	0.83 ± 0.01	1	0.83 ± 0.01	-	1.1 ± 0.2
A155	0.89 ± 0.01	1	0.89 ± 0.01	-	-
F156	0.85 ± 0.01	1	0.85 ± 0.01	-	-
Y157	0.85 ± 0.02	1	0.85 ± 0.02	-	1.5 ± 0.4
T158	0.83 ± 0.01	1	0.83 ± 0.01	-	2.2 ± 0.3
L159	0.89 ± 0.01	1	0.89 ± 0.01	-	-
V160			overlapping peaks		
R161	0.85 ± 0.02	1	0.85 ± 0.02	-	1.3 ± 0.4
E162	0.86 ± 0.01	1	0.86 ± 0.01	-	0.8 ± 0.3
I163	0.84 ± 0.01	1	0.84 ± 0.01	-	-
R164	N/A	N/A	N/A	N/A	N/A
K165	0.88 ± 0.01	1	0.88 ± 0.01	-	-
H166	N/A	N/A	N/A	N/A	N/A
K167	0.75 ± 0.02	0.88 ± 0.01	0.85 ± 0.01	799 ± 125	-
E168			overlapping peaks		
K169	N/A	N/A	N/A	N/A	N/A

Table S4 Backbone ^{15}N chemical shift differences between the ground and higher energy state ($|\Delta\delta_{EG}^{i}|$) as derived from a global fit analysis of CPMG relaxation dispersion measurements of the investigated GDP-bound K-Ras variants with parameters listed in Table 1 of the main text. P-loop (red), switch-I (orange) and switch-II (blue) are colored.

Res.	wt / ppm	G12C / ppm	G12D / ppm	G12V / ppm
M1	-	-	-	-
T2	-	-	-	-
E3	-	-	-	-
Y4	0.84 ± 0.08	1.53 ± 0.13	0.58 ± 0.05	0.87 ± 0.08
K5	1.75 ± 0.11	1.27 ± 0.11	1.11 ± 0.09	1.26 ± 0.11
L6	1.62 ± 0.13	-	1.50 ± 0.13	1.95 ± 0.16
V7	-	-	-	-
V8	-	-	0.94 ± 0.09	-
V9	1.25 ± 0.11	1.62 ± 0.13	1.17 ± 0.11	1.80 ± 0.14
G10	1.17 ± 0.10	1.16 ± 0.10	0.99 ± 0.09	1.27 ± 0.10
A11	0.75 ± 0.08	1.15 ± 0.10	0.76 ± 0.06	1.25 ± 0.10
V12	0.76 ± 0.08	1.46 ± 0.11	0.73 ± 0.06	-
G13	-	3.68 ± 0.29	1.33 ± 0.13	-
V14	-	0.70 ± 0.06	0.93 ± 0.09	-
G15	0.66 ± 0.05	-	0.91 ± 0.08	-
K16	1.33 ± 0.11	-	1.86 ± 0.18	-
S17	-	-	-	0.99 ± 0.09
A18	-	-	-	-
L19	-	-	-	-
T20	0.67 ± 0.06	0.91 ± 0.08	0.67 ± 0.06	1.21 ± 0.10
I21	0.78 ± 0.08	1.06 ± 0.10	-	-
Q22	0.84 ± 0.08	0.88 ± 0.08	0.76 ± 0.08	-
L23	-	-	-	-
I24	-	-	-	-
Q25	-	-	-	-
N26	-	-	-	-
H27	1.54 ± 0.13	2.06 ± 0.16	1.25 ± 0.11	2.78 ± 0.24
F28	-	-	-	-
V29	1.78 ± 0.15	2.07 ± 0.16	2.54 ± 0.23	1.69 ± 0.14
D30	0.67 ± 0.06	-	0.82 ± 0.08	-
E31	-	-	-	-
Y32	3.93 ± 0.35	4.64 ± 0.4	4.54 ± 0.39	3.10 ± 0.2
D33	3.60 ± 0.26	-	3.77 ± 0.33	3.01 ± 0.26
P34	-	-	-	-
T35	4.74 ± 0.4	3.32 ± 0.26	3.67 ± 0.33	4.59 ± 0.4
I36	1.77 ± 0.15	1.82 ± 0.15	2.16 ± 0.19	1.43 ± 0.13
E37	8.27 ± 0.65	-	-	-
D38	3.91 ± 0.34	4.39 ± 0.39	4.24 ± 0.36	3.47 ± 0.31
S39	0.77 ± 0.08	0.96 ± 0.09	0.62 ± 0.06	1.69 ± 0.15
Y40	2.11 ± 0.14	2.64 ± 0.24	2.36 ± 0.2	1.82 ± 0.15
R41	-	-	0.55 ± 0.05	-
K42	-	-	-	0.99 ± 0.09
Q43	-	-	-	0.95 ± 0.08

V44	-	-	-	-
V45	-	-	-	-
I46	-	-	-	-
D47	-	-	-	-
G48	-	-	-	-
E49	-	-	-	-
T50	-	-	-	-
C51	-	-	-	-
L52	0.97 ± 0.09	0.77 ± 0.08	0.65 ± 0.06	1.57 ± 0.13
L53	0.58 ± 0.05	-	-	0.84 ± 0.06
D54	0.97 ± 0.09	1.25 ± 0.1	0.92 ± 0.08	1.02 ± 0.09
I55	0.69 ± 0.06	1.53 ± 0.13	1.04 ± 0.09	1.15 ± 0.10
L56	1.64 ± 0.14	-	1.91 ± 0.18	2.27 ± 0.19
D57	-	-	6.25 ± 0.54	3.21 ± 0.26
T58	3.61 ± 0.26	4.44 ± 0.38	4.00 ± 0.36	2.25 ± 0.21
A59	2.05 ± 0.14	2.79 ± 0.23	3.02 ± 0.26	1.89 ± 0.18
G60	0.93 ± 0.08	1.36 ± 0.11	2.12 ± 0.19	-
Q61	0.57 ± 0.06	-	0.61 ± 0.05	1.34 ± 0.11
E62	1.24 ± 0.11	1.82 ± 0.14	2.24 ± 0.19	1.97 ± 0.16
E63	0.77 ± 0.08	-	-	-
Y64	2.06 ± 0.19	2.51 ± 0.21	2.27 ± 0.18	2.11 ± 0.18
S65	1.45 ± 0.13	0.64 ± 0.06	2.34 ± 0.21	0.71 ± 0.08
A66	3.85 ± 0.31	-	-	-
M67	1.27 ± 0.11	0.93 ± 0.08	0.61 ± 0.06	1.03 ± 0.09
R68	0.86 ± 0.08	1.29 ± 0.11	0.67 ± 0.06	0.99 ± 0.1
D69	0.80 ± 0.08	-	-	0.72 ± 0.06
Q70	-	1.16 ± 0.10	0.76 ± 0.08	1.18 ± 0.11
Y71	-	-	1.57 ± 0.14	-
M72	1.33 ± 0.10	-	1.58 ± 0.14	-
R73	1.64 ± 0.14	4.32 ± 0.34	1.27 ± 0.13	1.78 ± 0.19
T74	3.7 ± 0.26	3.41 ± 0.39	3.09 ± 0.24	2.66 ± 0.21
G75	4.05 ± 0.35	3.86 ± 0.31	3.71 ± 0.31	3.01 ± 0.24
E76	1.64 ± 0.14	-	0.72 ± 0.06	1.06 ± 0.09
G77	-	-	0.95 ± 0.10	-
F78	0.85 ± 0.08	-	-	-
L79	1.46 ± 0.13	1.97 ± 0.16	1.38 ± 0.13	2.12 ± 0.18
C80	-	-	-	-
V81	-	-	-	-
F82	0.65 ± 0.06	-	-	-
A83	-	-	-	-
I84	-	-	-	-
N85	-	-	-	-
N86	-	-	-	-
T87	-	-	-	-
K88	-	-	-	-
S89	-	-	-	-

F90	-	-	-	-
E91	-	-	-	-
D92	-	-	-	-
I93	-	-	-	-
H94	0.77 ± 0.08	-	-	-
H95	-	-	-	-
Y96	-	-	-	-
R97	0.96 ± 0.08	-	0.57 ± 0.05	0.68 ± 0.06
E98	-	-	-	-
Q99	-	0.93 ± 0.08	0.39 ± 0.04	1.00 ± 0.09
I100	-	-	-	-
K101	0.88 ± 0.08	-	0.97 ± 0.09	0.92 ± 0.08
R102	-	-	-	-
V103	-	-	-	-
K104	0.77 ± 0.08	-	0.67 ± 0.06	1.00 ± 0.09
D105	-	-	-	-
S106	-	-	-	-
E107	-	-	-	-
D108	-	-	-	-
V109	-	-	-	-
P110	-	-	-	-
M111	-	-	-	-
V112	-	-	0.48 ± 0.04	0.89 ± 0.06
L113	-	-	-	-
V114	-	-	-	-
G115	-	-	-	-
N116	-	-	-	-
K117	-	-	-	-
C118	-	-	-	-
D119	-	-	-	-
L120	-	-	-	-
P121	-	-	-	-
S122	-	-	-	-
R123	-	-	-	-
T124	-	-	-	0.89 ± 0.08
V125	-	-	-	-
D126	-	-	-	-
T127	-	-	-	-
K128	-	-	-	-
Q129	-	-	-	-
A130	-	-	-	-
Q131	-	-	-	-
D132	-	-	-	-
L133	-	-	-	-
A134	-	-	-	-
R135	-	-	-	-

S136	-	-	-	-
Y137	-	-	-	-
G138	-	-	-	-
I139	-	-	-	-
P140	-	-	-	-
F141	0.82 ± 0.08	-	-	-
I142	-	-	-	-
E143	-	-	0.61 ± 0.06	-
T144	-	-	-	-
S145	-	-	-	-
A146	-	-	0.82 ± 0.08	-
K147	-	-	-	-
T148	-	-	-	-
R149	-	0.91 ± 0.08	0.97 ± 0.09	1.29 ± 0.10
Q150	-	-	-	-
G151	-	-	-	-
V152	-	-	-	-
D153	-	-	-	-
D154	-	-	-	-
A155	-	-	-	-
F156	0.68 ± 0.06	0.76 ± 0.08	-	-
Y157	-	-	-	-
T158	-	-	-	-
L159	-	-	-	-
V160	0.78 ± 0.08	1.13 ± 0.09	0.84 ± 0.08	0.87 ± 0.08
R161	-	-	-	-
E162	-	-	-	-
I163	-	-	-	-
R164	-	-	-	-
K165	-	-	-	-
H166	-	-	-	-
K167	-	-	-	-
E168	0.80 ± 0.06	-	0.53 ± 0.05	-
K169	-	-	-	-

Table S5 Exchange parameters derived from ^{15}N-CEST measurements for wt, G12C, G12D, and G12V K-Ras·Mg^{2+}·GDP

Res.	**wt K-Ras·Mg^{2+}·GDP**		**G12C K-Ras·Mg^{2+}·GDP**		**G12D K-Ras·Mg^{2+}·GDP**		**G12V K-Ras·Mg^{2+}·GDP**	
	k_{ex} = 267 ± 20, p_E = 3.8 ± 0.1 %		k_{ex} = 214 ± 61, p_E = 1.3 ± 0.1 %		k_{ex} = 668 ± 60, p_E = 2.0 ± 0.1 %		k_{ex} = 492 ± 56, p_E = 1.5 ± 0.1 %	
	^{15}N δ/ppm	*^{15}N Δδ/ppm*	*^{15}N δ/ppm*	*^{15}N Δδ/ppm*	*^{15}N δ/ppm*	*^{15}N Δδ/ppm*	*^{15}N δ/ppm*	*^{15}N Δδ/ppm*
Y32	125.70	-4.35 ± 0.06	-	-	125.66	-4.49 ± 0.11	126.30	-5.11 ± 0.11
D33	128.91	-3.62 ± 0.08	-	-	128.61	-3.70 ± 0.14	-	-
T35	110.04	3.24 ± 0.08	109.46	3.73 ± 0.13	-	-	-	-
E37	132.06	-7.93 ± 0.07	132.89	-8.77 ± 0.12	131.95	-7.95 ± 0.24	132.93	-8.95 ± 0.11
D38	124.50	-4.22 ± 0.05	124.99	-4.77 ± 0.10	124.32	-4.11 ± 0.12	124.97	-5.00 ± 0.08
D57	129.25	-7.27 ± 0.06	-	-	129.14	-7.12 ± 0.15	-	-
T58	110.24	3.69 ± 0.07	109.73	4.27 ± 0.12	-	-	-	-
Y64	121.22	-2.89 ± 0.06	-	-	-	-	-	-
T74	108.03	2.39 ± 0.09	-	-	108.03	2.57 ± 0.23	107.90	2.05 ± 0.31
G75	111.24	-3.75 ± 0.06	-	-	111.34	-4.03 ± 0.12	111.58	-4.02 ± 0.10

Table S6 Backbone ^{15}N chemical shift differences between the ground and higher energy state ($|\Delta\delta_{EG}^{i}|$) as derived from a global fit analysis of CPMG relaxation dispersion measurements of the investigated GTP-bound K-Ras variants with parameters listed in Table 1 of the main text. Unassigned residues due to severe exchange broadening are marked with stars. P-loop (red), switch-I (orange) and switch-II (blue) are colored.

Res.	wt / ppm	G12C / ppm	G12D / ppm	G12V / ppm
M1	-	-	-	-
T2	0.27 ± 0.03	0.39 ± 0.04	0.32 ± 0.03	-
E3	-	-	-	-
Y4	-	-	-	0.60 ± 0.06
K5	-	-	-	-
L6	0.48 ± 0.05	0.67 ± 0.06	0.64 ± 0.06	1.04 ± 0.10
V7	0.49 ± 0.04	0.64 ± 0.06	0.30 ± 0.03	0.77 ± 0.08
V8	***	***	***	***
V9	0.99 ± 0.08	1.10 ± 0.10	0.89 ± 0.08	1.47 ± 0.13
G10	-	-	-	-
A11	***	***	***	***
V12	0.78 ± 0.06	1.53 ± 0.14	***	0.32 ± 0.03
G13	***	-	-	-
V14	0.54 ± 0.05	0.64 ± 0.06	0.44 ± 0.04	0.87 ± 0.08
G15	-	-	-	-
K16	-	-	0.57 ± 0.05	-
S17	1.16 ± 0.1	1.10 ± 0.10	0.54 ± 0.05	1.82 ± 0.16
A18	-	-	-	-
L19	0.43 ± 0.04	-	-	0.79 ± 0.08
T20	0.80 ± 0.07	1.01 ± 0.09	0.69 ± 0.06	1.20 ± 0.10
I21	0.79 ± 0.08	0.86 ± 0.08	-	-
Q22	***	***	***	***
L23	0.51 ± 0.05	0.63 ± 0.05	-	0.79 ± 0.07
I24	-	-	-	-
Q25	0.45 ± 0.04	-	-	0.91 ± 0.08
N26	0.55 ± 0.05	0.65 ± 0.05	0.30 ± 0.03	0.92 ± 0.08
H27	-	-	-	-
F28	0.53 ± 0.03	0.71 ± 0.06	0.64 ± 0.06	0.59 ± 0.05
V29	2.68 ± 0.23	3.00 ± 0.26	-	-
D30	***	***	***	***
E31	***	***	***	***
Y32	1.49 ± 0.14	1.96 ± 0.18	1.87 ± 0.18	3.88 ± 0.35
D33	***	***	***	***
P34	-	-	-	-
T35	-	2.30 ± 0.21	-	-
I36	***	***	***	***
E37	***	***	***	***
D38	***	***	***	***
S39	1.37 ± 0.13	1.50 ± 0.13	-	-
Y40	1.56 ± 0.14	1.50 ± 0.14	0.38 ± 0.05	0.74 ± 0.08
R41	0.42 ± 0.04	-	-	-
K42	-	-	-	0.68 ± 0.06

Q43	0.63 ± 0.05	0.64 ± 0.06	0.67 ± 0.06	0.73 ± 0.07
V44	0.43 ± 0.05	-	0.41 ± 0.04	0.69 ± 0.06
V45	0.52 ± 0.05	0.55 ± 0.06	0.5 ± 0.04	0.85 ± 0.08
I46	-	-	-	-
D47	-	-	-	-
G48	-	-	-	-
E49	-	-	-	0.41 ± 0.04
T50	-	-	-	-
C51	0.54 ± 0.06	0.71 ± 0.06	0.60 ± 0.06	0.83 ± 0.08
L52	0.63 ± 0.05	0.68 ± 0.06	0.62 ± 0.06	1.03 ± 0.09
L53	-	-	-	-
D54	***	***	***	***
I55	***	***	***	***
L56	***	***	***	***
D57	***	***	***	***
T58	***	***	***	***
A59	***	***	***	***
G60	***	***	***	***
Q61	***	***	***	***
E62	***	***	***	***
E63	***	***	***	***
Y64	***	***	***	***
S65	***	***	***	***
A66	***	***	***	***
M67	***	***	***	***
R68	***	***	***	***
D69	***	***	***	***
Q70	***	***	***	***
Y71	***	***	***	***
M72	***	***	***	***
R73	***	***	***	***
T74	0.81 ± 0.08	1.04 ± 0.09	1.20 ± 0.11	1.66 ± 0.15
G75	0.51 ± 0.05	-	0.84 ± 0.07	-
E76	-	-	-	0.45 ± 0.03
G77	-	-	-	0.51 ± 0.03
F78	-	-	0.47 ± 0.04	0.47 ± 0.03
L79	-	1.15 ± 0.09	-	2.15 ± 0.18
C80	0.45 ± 0.04	0.56 ± 0.05	0.54 ± 0.04	0.63 ± 0.06
V81	-	0.46 ± 0.04	-	-
F82	-	-	-	-
A83	-	-	-	-
I84	-	-	-	-
N85	-	-	-	0.42 ± 0.03
N86	-	-	-	-
T87	***	***	***	***
K88	-	-	-	-

S89	0.30 ± 0.03	0.46 ± 0.04	0.48 ± 0.04	0.6 ± 0.06
F90	0.56 ± 0.05	0.50 ± 0.05	0.57 ± 0.06	0.59 ± 0.05
E91	-	0.88 ± 0.08	-	0.52 ± 0.04
D92	0.51 ± 0.05	0.55 ± 0.05	0.80 ± 0.08	0.85 ± 0.08
I93	1.01 ± 0.1	0.91 ± 0.08	-	1.58 ± 0.14
H94	0.71 ± 0.06	-	0.89 ± 0.08	-
H95	0.79 ± 0.07	0.81 ± 0.08	0.85 ± 0.08	1.20 ± 0.10
Y96	1.22 ± 0.10	-	0.38 ± 0.03	0.64 ± 0.05
R97	0.41 ± 0.03	0.78 ± 0.06	0.19 ± 0.03	0.43 ± 0.04
E98	0.76 ± 0.07	0.65 ± 0.06	0.27 ± 0.03	1.16 ± 0.10
Q99	-	-	***	-
I100	***	-	***	-
K101	0.51 ± 0.04	0.41 ± 0.04	***	0.77 ± 0.06
R102	0.61 ± 0.05	0.54 ± 0.05	***	1.01 ± 0.09
V103	***	***	***	***
K104	-	-	-	-
D105	-	-	-	-
S106	-	-	-	-
E107	-	-	-	-
D108	-	-	-	-
V109	-	-	-	-
P110	-	-	-	-
M111	0.40 ± 0.04	0.62 ± 0.06	-	0.97 ± 0.08
V112	***	0.56 ± 0.05	-	0.56 ± 0.05
L113	0.48 ± 0.05	0.46 ± 0.04	0.56 ± 0.06	0.73 ± 0.06
V114	0.76 ± 0.07	0.47 ± 0.04	0.59 ± 0.05	0.68 ± 0.05
G115	-	-	-	-
N116	-	0.42 ± 0.04	-	-
K117	-	-	-	-
C118	-	-	-	-
D119	0.46 ± 0.04	0.40 ± 0.04	-	0.68 ± 0.05
L120	-	-	-	-
P121	-	-	-	-
S122	-	-	-	-
R123	-	-	-	-
T124	-	-	-	-
V125	-	-	-	-
D126	-	-	-	-
T127	-	-	-	-
K128	-	-	-	-
Q129	-	-	-	-
A130	-	-	-	0.52 ± 0.04
Q131	0.41 ± 0.04	-	0.27 ± 0.03	0.52 ± 0.03
D132	-	-	-	-
L133	-	-	-	-
A134	-	-	-	-

R135	0.46 ± 0.03	-	-	-
S136	-	-	-	-
Y137	-	-	-	0.40 ± 0.03
G138	-	-	-	-
I139	-	-	-	-
P140	-	-	-	-
F141	0.55 ± 0.04	-	0.29 ± 0.02	0.40 ± 0.03
I142	-	-	-	-
E143	-	-	-	0.39 ± 0.03
T144	0.55 ± 0.05	-	0.42 ± 0.03	0.84 ± 0.07
S145	-	-	-	-
A146	-	-	-	-
K147	0.48 ± 0.04	0.41 ± 0.03	0.36 ± 0.04	-
T148	-	-	-	-
R149	0.87 ± 0.08	1.00 ± 0.10	0.59 ± 0.05	1.53 ± 0.12
Q150	-	-	-	-
G151	-	-	-	-
V152	0.46 ± 0.04	-	0.50 ± 0.06	0.67 ± 0.06
D153	0.30 ± 0.03	-	0.58 ± 0.07	-
D154	-	-	-	-
A155	-	-	-	-
F156	-	-	-	0.39 ± 0.03
Y157	0.4 ± 0.04	0.49 ± 0.05	0.46 ± 0.04	0.56 ± 0.05
T158	-	-	-	-
L159	0.29 ± 0.04	-	-	0.46 ± 0.03
V160	-	-	-	-
R161	0.51 ± 0.04	0.66 ± 0.07	0.52 ± 0.05	1.16 ± 0.10
E162	-	-	-	-
I163	-	-	-	-
R164	0.41 ± 0.04	-	0.47 ± 0.04	-
K165	0.43 ± 0.04	0.44 ± 0.04	-	0.72 ± 0.06
H166	-	-	-	-
K167	-	-	-	-
E168	-	-	-	0.31 ± 0.04
K169	-	-	-	-

Table S7 Experimental fast dynamics parameters (R_1, R_2, R_2/R_1 and ^{15}N-{^1H} HetNOE) of Mg^{2+}-free K-Ras-G12C·bound GDP recorded at 700 MHz at 298 K. P-loop (red), switch-I (orange) and switch-II (blue) are colored.

Res.	Mg^{2+}-free K-Ras-G12C-GDP			
	R_1 / s^{-1}	R_2 / s^{-1}	R_2 / R_1	^{15}N-{^1H} NOE
M1				
T2	1.11 ± 0.03	9.8 ± 0.8	8.8 ± 0.7	0.52
E3	0.96 ± 0.01	14.0 ± 0.4	14.7 ± 0.4	0.67
Y4	0.90 ± 0.02	13.3 ± 0.5	14.9 ± 0.6	0.83
K5	0.85 ± 0.02	12.4 ± 0.3	14.5 ± 0.5	0.79
L6	0.86 ± 0.02	14.7 ± 0.5	17.1 ± 0.7	0.78
V7	overlapping peaks			
V8	0.98 ± 0.03	15.0 ± 0.5	15.3 ± 0.7	0.83
V9	0.98 ± 0.01	17.2 ± 0.7	17.5 ± 0.8	0.89
G10	0.95 ± 0.02	15.8 ± 0.2	16.7 ± 0.5	0.79
A11	0.94 ± 0.04	13.7 ± 0.9	14.6 ± 1.1	0.92
C12	0.96 ± 0.02	14.3 ± 0.6	14.9 ± 0.7	0.80
G13	0.91 ± 0.04	15.5 ± 1.2	17.1 ± 1.5	0.82
V14	0.98 ± 0.01	13.7 ± 0.5	14.0 ± 0.6	0.78
G15	0.99 ± 0.02	14.3 ± 0.9	14.5 ± 1.0	0.87
K16	0.95 ± 0.01	15.3 ± 0.8	16.2 ± 0.9	0.81
S17	0.89 ± 0.02	14.7 ± 0.9	16.6 ± 1.1	0.84
A18	0.90 ± 0.03	14.6 ± 0.6	16.2 ± 0.9	0.88
L19	0.95 ± 0.03	16.3 ± 0.2	17.2 ± 0.6	0.84
T20	0.91 ± 0.03	15.2 ± 0.6	16.6 ± 0.8	0.81
I21	0.94 ± 0.03	13.0 ± 0.6	13.8 ± 0.8	0.84
Q22	1.03 ± 0.02	21.0 ± 0.5	20.3 ± 0.7	0.80
L23	0.93 ± 0.02	14.4 ± 0.4	15.5 ± 0.6	0.81
I24	0.96 ± 0.01	17.5 ± 0.4	18.1 ± 0.5	0.89
Q25	0.96 ± 0.04	16.3 ± 1.4	17.1 ± 1.6	0.81
N26	0.99 ± 0.01	15.4 ± 0.6	15.6 ± 0.6	0.83
H27	N/A	N/A	N/A	N/A
F28	0.95 ± 0.05	13.8 ± 0.9	14.6 ± 1.2	0.69
V29	1.13 ± 0.02	22.9 ± 0.6	20.2 ± 0.6	0.63
D30	0.99 ± 0.02	10.5 ± 0.8	10.5 ± 0.8	0.48
E31	overlapping peaks			
Y32	1.22 ± 0.03	9.9 ± 0.4	8.2 ± 0.4	0.46
D33	1.15 ± 0.03	10.2 ± 0.5	8.9 ± 0.5	0.58
P34	N/A	N/A	N/A	N/A
T35	1.17 ± 0.03	11.1 ± 0.2	9.5 ± 0.3	0.53
I36	1.25 ± 0.04	10.8 ± 0.4	8.6 ± 0.4	0.61
E37	1.26 ± 0.03	9.2 ± 0.5	7.3 ± 0.4	0.52
D38	1.23 ± 0.02	9.1 ± 0.4	7.4 ± 0.3	0.49
S39	1.17 ± 0.03	9.6 ± 0.4	8.2 ± 0.4	0.54
Y40	1.17 ± 0.02	11.3 ± 1.0	9.7 ± 0.8	0.62
R41	overlapping peaks			
K42	0.93 ± 0.02	12.5 ± 0.1	13.6 ± 0.3	0.75

Q43	0.93 ± 0.03	15.5 ± 0.9	16.6 ± 1.1	0.83
V44	0.94 ± 0.02	14.5 ± 0.5	15.4 ± 0.7	0.84
V45	0.96 ± 0.01	12.8 ± 0.3	13.4 ± 0.4	0.73
I46	0.86 ± 0.02	14.6 ± 0.7	17.0 ± 0.9	0.78
D47	N/A	N/A	N/A	N/A
G48	0.91 ± 0.06	13.9 ± 1.8	15.2 ± 2.3	0.77
E49	0.95 ± 0.02	13.5 ± 0.5	14.3 ± 0.6	0.78
T50	0.91 ± 0.04	14.8 ± 1.4	16.2 ± 1.7	0.78
C51	0.99 ± 0.02	13.8 ± 0.3	14.0 ± 0.4	0.84
L52	0.90 ± 0.02	13.0 ± 0.3	14.4 ± 0.4	0.77
L53	0.88 ± 0.02	14.3 ± 1	16.1 ± 1.2	0.79
D54	overlapping peaks			
I55	0.84 ± 0.01	12.7 ± 0.9	15.2 ± 1.0	0.75
L56	0.93 ± 0.02	15.3 ± 0.6	16.4 ± 0.7	0.85
D57	0.94 ± 0.04	17.6 ± 1.1	18.7 ± 1.4	0.66
T58	overlapping peaks			
A59	1.04 ± 0.01	14.0 ± 0.7	13.4 ± 0.7	0.74
G60	1.14 ± 0.08	15.0 ± 2.0	13.1 ± 2.0	0.61
Q61	1.09 ± 0.02	13.0 ± 0.5	11.9 ± 0.6	0.69
E62	0.91 ± 0.09	13.6 ± 1.4	14.9 ± 2.1	0.66
E63	1.14 ± 0.04	14.0 ± 0.6	12.3 ± 0.7	0.58
Y64	overlapping peaks			
S65	N/A	N/A	N/A	N/A
A66	N/A	N/A	N/A	N/A
M67	0.95 ± 0.03	14.4 ± 1.3	15.2 ± 1.5	0.71
R68	overlapping peaks			
D69	1.01 ± 0.02	13.7 ± 0.7	13.5 ± 0.8	0.73
Q70	overlapping peaks			
Y71	1.02 ± 0.04	15.7 ± 0.8	15.4 ± 1.0	0.78
M72	1.06 ± 0.04	17.4 ± 0.3	16.4 ± 0.6	0.78
R73	overlapping peaks			
T74	0.98 ± 0.04	16.8 ± 0.7	17.1 ± 1.0	0.76
G75	1.00 ± 0.02	15.8 ± 0.2	15.8 ± 0.3	0.86
E76	0.95 ± 0.02	13.8 ± 0.2	14.5 ± 0.4	0.86
G77	0.90 ± 0.01	12.7 ± 0.6	14.1 ± 0.6	0.81
F78	0.97 ± 0.05	12.0 ± 0.3	12.4 ± 0.7	0.85
L79	0.94 ± 0.02	14.8 ± 0.4	15.8 ± 0.5	0.86
C80	0.88 ± 0.01	13.6 ± 0.1	15.4 ± 0.3	0.76
V81	0.89 ± 0.03	14.9 ± 0.3	16.9 ± 0.6	0.82
F82	0.97 ± 0.01	13.3 ± 0.3	13.7 ± 0.3	0.88
A83	1.01 ± 0.03	13.4 ± 0.8	13.3 ± 0.9	0.78
I84	0.90 ± 0.02	15.6 ± 1.0	17.2 ± 1.1	0.84
N85	0.97 ± 0.01	15.8 ± 0.6	16.4 ± 0.6	0.90
N86	overlapping peaks			
T87	N/A	N/A	N/A	N/A
K88	0.98 ± 0.03	14.6 ± 0.7	14.9 ± 0.9	0.84

S89		overlapping peaks		
F90	0.94 ± 0.03	15.6 ± 0.4	16.7 ± 0.7	0.77
E91	0.90 ± 0.02	14.8 ± 0.5	16.4 ± 0.7	0.86
D92	0.90 ± 0.01	13.9 ± 0.3	15.4 ± 0.4	0.84
I93	0.91 ± 0.03	14.2 ± 0.9	15.6 ± 1.1	0.75
H94	0.93 ± 0.03	15.4 ± 1.5	16.6 ± 1.6	0.80
H95	0.95 ± 0.01	13.6 ± 0.3	14.4 ± 0.3	0.81
Y96	0.91 ± 0.02	15.7 ± 0.8	17.2 ± 0.9	0.87
R97	0.91 ± 0.01	15.3 ± 0.5	16.9 ± 0.6	0.73
E98	0.89 ± 0.02	14.7 ± 0.6	16.4 ± 0.8	0.73
Q99		overlapping peaks		
I100	0.93 ± 0.01	15.2 ± 0.4	16.3 ± 0.5	0.83
K101	0.93 ± 0.01	14.7 ± 0.3	15.7 ± 0.4	0.86
R102	0.93 ± 0.01	15.4 ± 0.2	16.6 ± 0.3	0.73
V103	0.95 ± 0.01	15.3 ± 0.3	16.1 ± 0.4	0.76
K104	0.95 ± 0.01	14.5 ± 0.3	15.2 ± 0.4	0.79
D105	0.99 ± 0.03	13.3 ± 0.6	13.5 ± 0.7	0.74
S106	0.97 ± 0.02	13.6 ± 0.3	13.9 ± 0.5	0.75
E107	0.90 ± 0.07	11.2 ± 0.6	12.4 ± 1.2	0.56
D108	0.96 ± 0.03	11.1 ± 0.7	11.6 ± 0.8	0.52
V109	0.98 ± 0.03	9.4 ± 0.3	9.5 ± 0.5	0.43
P110	N/A	N/A	N/A	N/A
M111	0.94 ± 0.02	13.9 ± 0.4	14.7 ± 0.5	0.84
V112	0.95 ± 0.03	14.2 ± 0.4	14.9 ± 0.6	0.73
L113	0.97 ± 0.02	14.8 ± 0.2	15.3 ± 0.3	0.84
V114	0.96 ± 0.02	15.3 ± 0.3	15.9 ± 0.4	0.80
G115	0.91 ± 0.02	13.7 ± 0.3	15.1 ± 0.4	0.83
N116	0.91 ± 0.01	13.4 ± 0.6	14.8 ± 0.7	0.85
K117	0.96 ± 0.02	16.4 ± 3.1	17.2 ± 3.3	0.80
C118	0.92 ± 0.01	14.8 ± 0.6	16.0 ± 0.7	0.84
D119	1.03 ± 0.02	15.7 ± 0.8	15.3 ± 0.8	0.81
L120	0.95 ± 0.01	14.5 ± 0.8	15.2 ± 0.8	0.81
P121	N/A	N/A	N/A	N/A
S122	0.87 ± 0.03	11.6 ± 0.5	13.5 ± 0.8	0.69
R123		overlapping peaks		
T124	0.89 ± 0.04	14.0 ± 0.8	15.8 ± 1.1	0.82
V125	0.89 ± 0.02	12.8 ± 0.7	14.5 ± 0.9	0.74
D126	0.98 ± 0.01	13.7 ± 0.8	14.0 ± 0.8	0.74
T127	0.94 ± 0.02	13.3 ± 0.7	14.1 ± 0.8	0.84
K128	1.02 ± 0.02	14.1 ± 0.3	13.8 ± 0.4	0.77
Q129	0.94 ± 0.01	13.9 ± 0.4	14.7 ± 0.5	0.73
A130	0.97 ± 0.01	14.2 ± 0.2	14.7 ± 0.2	0.82
Q131	0.94 ± 0.04	15.1 ± 0.3	16.0 ± 0.8	0.77
D132	0.90 ± 0.02	14.4 ± 0.3	15.9 ± 0.4	0.82
L133	0.96 ± 0.01	14.3 ± 0.4	14.8 ± 0.4	0.77
A134	0.94 ± 0.01	14.1 ± 0.3	15.1 ± 0.3	0.92

R135	0.95 ± 0.01	15.6 ± 0.2	16.4 ± 0.2	0.77
S136	0.88 ± 0.02	14.6 ± 0.3	16.5 ± 0.5	0.78
Y137	0.87 ± 0.01	13.7 ± 0.3	15.9 ± 0.4	0.84
G138	0.92 ± 0.01	13.6 ± 0.2	14.8 ± 0.2	0.85
I139	0.9 ± 0.01	14.5 ± 0.6	16.0 ± 0.7	0.84
P140	N/A	N/A	N/A	N/A
F141	0.91 ± 0.01	13.4 ± 0.2	14.8 ± 0.2	0.77
I142	0.94 ± 0.01	13.5 ± 0.4	14.4 ± 0.5	0.81
E143	0.87 ± 0.01	13.1 ± 0.1	15.1 ± 0.2	0.81
T144	0.94 ± 0.03	13.9 ± 0.6	14.8 ± 0.8	0.86
S145	0.85 ± 0.03	13.2 ± 0.2	15.5 ± 0.5	0.87
A146	0.92 ± 0.04	14.5 ± 1.0	15.7 ± 1.3	0.86
K147	0.90 ± 0.02	14.9 ± 0.4	16.4 ± 0.6	0.83
T148	0.91 ± 0.03	16.2 ± 1.6	17.8 ± 1.9	0.85
R149	overlapping peaks			
Q150	0.86 ± 0.02	13.9 ± 0.9	16.2 ± 1.1	0.68
G151	0.97 ± 0.04	13.7 ± 0.6	14.2 ± 0.9	0.78
V152	0.98 ± 0.01	14.6 ± 0.5	14.9 ± 0.5	0.90
D153	0.93 ± 0.02	14.5 ± 0.4	15.5 ± 0.5	0.85
D154	overlapping peaks			
A155	overlapping peaks			
F156	0.93 ± 0.01	13.5 ± 0.8	14.5 ± 0.8	0.76
Y157	0.90 ± 0.01	15.3 ± 0.5	17.0 ± 0.5	0.88
T158	0.90 ± 0.01	15.5 ± 0.4	17.2 ± 0.5	0.83
L159	0.94 ± 0.02	14.6 ± 0.3	15.4 ± 0.5	0.84
V160	0.91 ± 0.02	14.6 ± 0.6	16.0 ± 0.7	0.88
R161	0.95 ± 0.02	14.9 ± 0.8	15.7 ± 0.9	0.77
E162	0.92 ± 0.03	15.4 ± 0.1	16.7 ± 0.6	0.80
I163	0.97 ± 0.02	14.4 ± 0.7	14.9 ± 0.8	0.83
R164	0.92 ± 0.02	15.2 ± 0.3	16.5 ± 0.4	0.88
K165	0.94 ± 0.01	14.5 ± 0.3	15.4 ± 0.4	0.77
H166	overlapping peaks			
K167	overlapping peaks			
E168	1.07 ± 0.03	10.2 ± 0.4	9.5 ± 0.5	0.50
K169	1.24 ± 0.01	5.9 ± 0.3	4.8 ± 0.2	0.05

Table S8 Extended model-free parameters (S^2, S^2_s, S^2_f, τ_e, R_{ex}) of Mg^{2+}-free K-Ras-G12C·bound GDP recorded at 700 MHz at 298 K. P-loop (red), switch-I (orange) and switch-II (blue) are colored.

Res.	Mg^{2+}-free K-Ras-G12C-GDP				
	S^2	S^2_s	S^2_f	τ_e / ps	R_{ex} / s^{-1}
M1	N/A	N/A	N/A	N/A	N/A
T2	0.54 ± 0.04	0.79 ± 0.04	0.69 ± 0.04	1000 ± 126	-
E3	0.83 ± 0.01	1	0.83 ± 0.01	42 ± 9	-
Y4	0.81 ± 0.02	1	0.81 ± 0.02	-	-
K5	0.76 ± 0.01	1	0.76 ± 0.01	-	-
L6	0.78 ± 0.02	1	0.78 ± 0.02	-	1.6 ± 0.6
V7			overlapping peaks		
V8	0.89 ± 0.02	1	0.89 ± 0.02	-	-
V9	0.89 ± 0.01	1	0.89 ± 0.01	-	2.3 ± 0.8
G10	0.86 ± 0.02	1	0.86 ± 0.02	-	1.4 ± 0.4
A11	0.84 ± 0.03	1	0.84 ± 0.03	-	-
C12	0.87 ± 0.02	1	0.87 ± 0.02	-	-
G13	0.85 ± 0.03	1	0.85 ± 0.03	-	-
V14	0.88 ± 0.01	1	0.88 ± 0.01	-	-
G15	0.89 ± 0.02	1	0.89 ± 0.02	-	-
K16	0.86 ± 0.01	1	0.86 ± 0.01	-	-
S17	0.82 ± 0.02	1	0.82 ± 0.02	-	-
A18	0.83 ± 0.02	1	0.83 ± 0.02	-	-
L19	0.86 ± 0.03	1	0.86 ± 0.03	-	1.9 ± 0.5
T20	0.85 ± 0.02	1	0.85 ± 0.02	-	-
I21	0.83 ± 0.02	1	0.83 ± 0.02	-	-
Q22	0.94 ± 0.02	1	0.94 ± 0.02	-	5.3 ± 0.6
L23	0.85 ± 0.02	1	0.85 ± 0.02	-	-
I24	0.87 ± 0.01	1	0.87 ± 0.01	-	2.8 ± 0.5
Q25	0.89 ± 0.04	1	0.89 ± 0.04	-	-
N26	0.90 ± 0.01	1	0.90 ± 0.01	-	-
H27	N/A	N/A	N/A	N/A	N/A
F28	0.82 ± 0.03	1	0.82 ± 0.03	34 ± 13	-
V29	0.91 ± 0.02	1	0.91 ± 0.02	482 ± 104	7.5 ± 0.7
D30	0.60 ± 0.04	0.79 ± 0.03	0.76 ± 0.04	745 ± 121	-
E31			overlapping peaks		
Y32	0.55 ± 0.03	0.85 ± 0.02	0.64 ± 0.02	954 ± 89	-
D33	0.57 ± 0.03	0.81 ± 0.03	0.7 ± 0.03	1116 ± 142	-
P34	N/A	N/A	N/A	N/A	N/A
T35	0.63 ± 0.02	0.87 ± 0.02	0.72 ± 0.02	948 ± 106	-
I36	0.60 ± 0.03	0.85 ± 0.03	0.70 ± 0.02	1252 ± 175	-
E37	0.49 ± 0.03	0.82 ± 0.03	0.60 ± 0.03	1132 ± 115	-
D38	0.49 ± 0.02	0.82 ± 0.02	0.60 ± 0.02	1075 ± 102	-
S39	0.53 ± 0.03	0.80 ± 0.02	0.66 ± 0.02	1094 ± 120	-
Y40	0.64 ± 0.05	0.85 ± 0.04	0.75 ± 0.04	1153 ± 198	-
R41			overlapping peaks		
K42	N/A	N/A	N/A	N/A	N/A

Q43	0.86 ± 0.02	1	0.86 ± 0.02	-	-
V44	0.86 ± 0.02	1	0.86 ± 0.02	-	-
V45	N/A	N/A	N/A	N/A	N/A
I46	0.79 ± 0.02	1	0.79 ± 0.02	-	-
D47	N/A	N/A	N/A	N/A	N/A
G48	0.83 ± 0.05	1	0.83 ± 0.05	-	-
E49	0.84 ± 0.02	1	0.84 ± 0.02	-	-
T50	0.84 ± 0.04	1	0.84 ± 0.04	-	-
C51	0.86 ± 0.01	1	0.86 ± 0.01	-	-
L52	0.79 ± 0.01	1	0.79 ± 0.01	-	-
L53	0.80 ± 0.01	1	0.80 ± 0.01	-	-
D54			overlapping peaks		
I55	0.76 ± 0.01	1	0.76 ± 0.01	-	-
L56	0.86 ± 0.02	1	0.86 ± 0.02	-	-
D57	0.81 ± 0.03	1	0.81 ± 0.03	39 ± 12	3.9 ± 1.3
T58			overlapping peaks		
A59	0.94 ± 0.01	1	0.94 ± 0.01	-	-
G60	0.89 ± 0.06	1	0.89 ± 0.06	537 ± 367	-
Q61	0.76 ± 0.03	0.88 ± 0.03	0.86 ± 0.02	1047 ± 246	-
E62	0.80 ± 0.06	1	0.80 ± 0.06	34 ± 15	-
E63	0.86 ± 0.03	1	0.86 ± 0.03	571 ± 136	-
Y64			overlapping peaks		
S65	N/A	N/A	N/A	N/A	N/A
A66	N/A	N/A	N/A	N/A	N/A
M67	0.83 ± 0.03	1	0.83 ± 0.03	32 ± 12	-
R68			overlapping peaks		
D69	0.90 ± 0.02	1	0.90 ± 0.02	-	-
Q70			overlapping peaks		
Y71	0.93 ± 0.03	1	0.93 ± 0.03	-	-
M72	1.00 ± 0.02	1	1.00 ± 0.02	-	-
R73			overlapping peaks		
T74	0.93 ± 0.03	1	0.93 ± 0.03	-	-
G75	0.92 ± 0.01	1	0.92 ± 0.01	-	-
E76	0.83 ± 0.01	1	0.83 ± 0.01	-	-
G77	0.81 ± 0.01	1	0.81 ± 0.01	-	-
F78	0.74 ± 0.02	1	0.74 ± 0.02	-	-
L79	0.86 ± 0.01	1	0.86 ± 0.01	-	-
C80	0.81 ± 0.01	1	0.81 ± 0.01	-	-
V81	0.80 ± 0.02	1	0.80 ± 0.02	-	1.5 ± 0.5
F82	N/A	N/A	N/A	N/A	N/A
A83	0.89 ± 0.02	1	0.89 ± 0.02	-	-
I84	0.83 ± 0.02	1	0.83 ± 0.02	-	-
N85	0.88 ± 0.01	1	0.88 ± 0.01	-	-
N86			overlapping peaks		
T87	N/A	N/A	N/A	N/A	N/A
K88	0.88 ± 0.02	1	0.88 ± 0.02	-	-

S89			overlapping peaks		
F90	0.88 ± 0.02	1	0.88 ± 0.02	-	-
E91	0.83 ± 0.01	1	0.83 ± 0.01	-	-
D92	0.82 ± 0.01	1	0.82 ± 0.01	-	-
I93	0.83 ± 0.03	1	0.83 ± 0.03	-	-
H94	0.85 ± 0.02	1	0.85 ± 0.02	-	-
H95	0.85 ± 0.01	1	0.85 ± 0.01	-	-
Y96	0.84 ± 0.01	1	0.84 ± 0.01	-	-
R97	0.83 ± 0.01	1	0.83 ± 0.01	-	-
E98	0.82 ± 0.02	1	0.82 ± 0.02	-	-
Q99			overlapping peaks		
I100	0.86 ± 0.01	1	0.86 ± 0.01	-	-
K101	0.85 ± 0.01	1	0.85 ± 0.01	-	-
R102	0.82 ± 0.01	1	0.82 ± 0.01	24 ± 9	1.7 ± 0.3
V103	0.87 ± 0.01	1	0.87 ± 0.01	-	-
K104	0.86 ± 0.01	1	0.86 ± 0.01	-	-
D105	0.85 ± 0.02	1	0.85 ± 0.02	-	-
S106	0.84 ± 0.01	1	0.84 ± 0.01	-	-
E107	N/A	N/A	N/A	N/A	N/A
D108	0.65 ± 0.04	0.79 ± 0.03	0.81 ± 0.03	669 ± 133	-
V109	0.53 ± 0.02	0.75 ± 0.02	0.71 ± 0.02	780 ± 80	-
P110	N/A	N/A	N/A	N/A	N/A
M111	0.85 ± 0.01	1	0.85 ± 0.01	-	-
V112	0.85 ± 0.02	1	0.85 ± 0.02	-	-
L113	0.88 ± 0.01	1	0.88 ± 0.01	-	-
V114	0.89 ± 0.01	1	0.89 ± 0.01	-	-
G115	0.82 ± 0.01	1	0.82 ± 0.01	-	-
N116	0.82 ± 0.01	1	0.82 ± 0.01	-	-
K117	0.87 ± 0.02	1	0.87 ± 0.02	-	-
C118	0.84 ± 0.01	1	0.84 ± 0.01	-	-
D119	0.93 ± 0.01	1	0.93 ± 0.01	-	-
L120	0.86 ± 0.01	1	0.86 ± 0.01	-	-
P121	N/A	N/A	N/A	N/A	N/A
S122	0.73 ± 0.02	1	0.73 ± 0.02	22 ± 6	-
R123			overlapping peaks		
T124	0.82 ± 0.03	1	0.82 ± 0.03	-	-
V125	0.8 ± 0.02	1	0.8 ± 0.02	-	-
D126	0.86 ± 0.01	1	0.86 ± 0.01	34 ± 12	-
T127	0.85 ± 0.02	1	0.85 ± 0.02	-	-
K128	0.89 ± 0.01	1	0.89 ± 0.01	-	-
Q129	0.83 ± 0.01	1	0.83 ± 0.01	28 ± 10	-
A130	0.87 ± 0.01	1	0.87 ± 0.01	-	-
Q131	0.89 ± 0.01	1	0.89 ± 0.01	-	-
D132	0.84 ± 0.01	1	0.84 ± 0.01	-	-
L133	0.87 ± 0.01	1	0.87 ± 0.01	-	-
A134	0.85 ± 0.01	1	0.85 ± 0.01	-	-

R135	0.86 ± 0.01	1	0.86 ± 0.01	-	1.2 ± 0.2
S136	0.83 ± 0.01	1	0.83 ± 0.01	-	-
Y137	0.80 ± 0.01	1	0.80 ± 0.01	-	-
G138	0.82 ± 0.01	1	0.82 ± 0.01	-	-
I139	0.82 ± 0.01	1	0.82 ± 0.01	-	-
P140	N/A	N/A	N/A	N/A	N/A
F141	0.80 ± 0.01	1	0.80 ± 0.01	18 ± 7	-
I142	0.85 ± 0.01	1	0.85 ± 0.01	-	-
E143	0.78 ± 0.01	1	0.78 ± 0.01	-	-
T144	0.84 ± 0.02	1	0.84 ± 0.02	-	-
S145	0.78 ± 0.01	1	0.78 ± 0.01	-	-
A146	0.84 ± 0.03	1	0.84 ± 0.03	-	-
K147	0.84 ± 0.02	1	0.84 ± 0.02	-	-
T148	0.83 ± 0.02	1	0.83 ± 0.02	-	-
R149			overlapping peaks		
Q150	0.78 ± 0.02	1	0.78 ± 0.02	-	-
G151	0.85 ± 0.03	1	0.85 ± 0.03	-	-
V152	0.88 ± 0.01	1	0.88 ± 0.01	-	-
D153	0.85 ± 0.02	1	0.85 ± 0.02	-	-
D154			overlapping peaks		
A155			overlapping peaks		
F156	0.84 ± 0.01	1	0.84 ± 0.01	-	-
Y157	0.82 ± 0.01	1	0.82 ± 0.01	-	1.6 ± 0.5
T158	0.82 ± 0.01	1	0.82 ± 0.01	-	1.8 ± 0.4
L159	0.86 ± 0.01	1	0.86 ± 0.01	-	-
V160	0.83 ± 0.01	1	0.83 ± 0.01	-	-
R161	0.86 ± 0.02	1	0.86 ± 0.02	-	-
E162	0.91 ± 0.01	1	0.91 ± 0.01	-	-
I163	0.87 ± 0.02	1	0.87 ± 0.02	-	-
R164	0.83 ± 0.01	1	0.83 ± 0.01	-	1.2 ± 0.3
K165	0.86 ± 0.01	1	0.86 ± 0.01	-	-
H166			overlapping peaks		
K167			overlapping peaks		
E168	0.58 ± 0.03	0.8 ± 0.02	0.72 ± 0.02	888 ± 99	-
K169	N/A	N/A	N/A	N/A	N/A

Supplementary figures

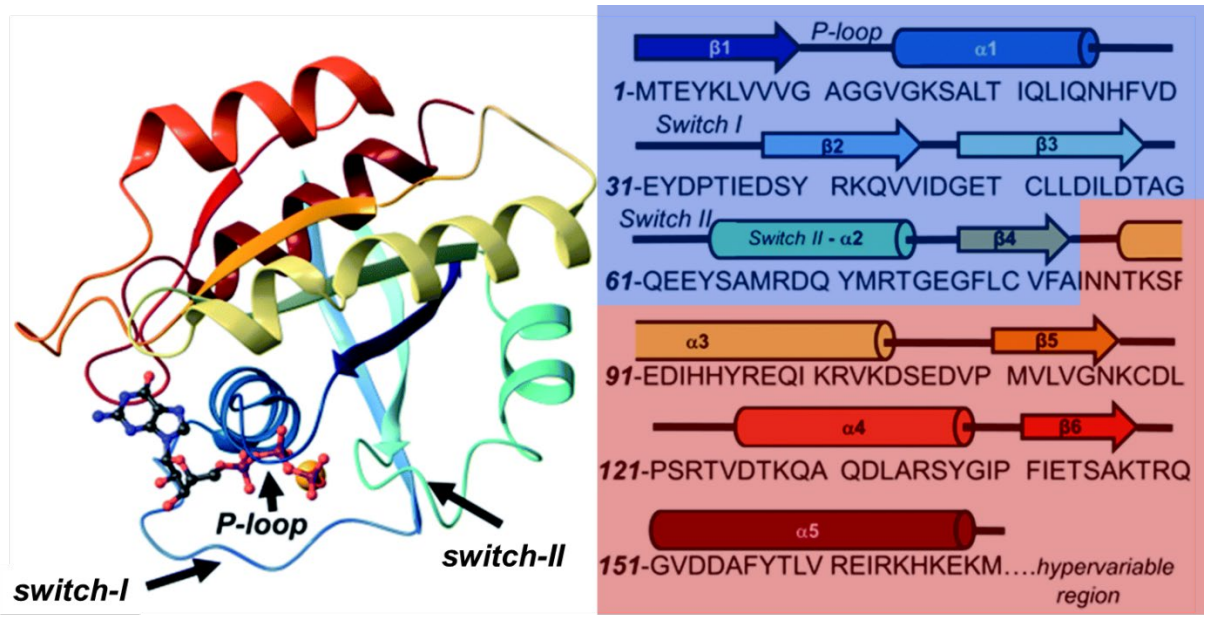

Figure S1 3D structure of GTP-bound G-domain of K-Ras-wt and its sequence showing the secondary structural elements. The effector lobe is colored blue (and secondary structure elements are shown in shades of blue) and the allosteric lobe is red (secondary structure elements are shown in shades of red). The structure is derived from our previous MD-simulation study.[2]

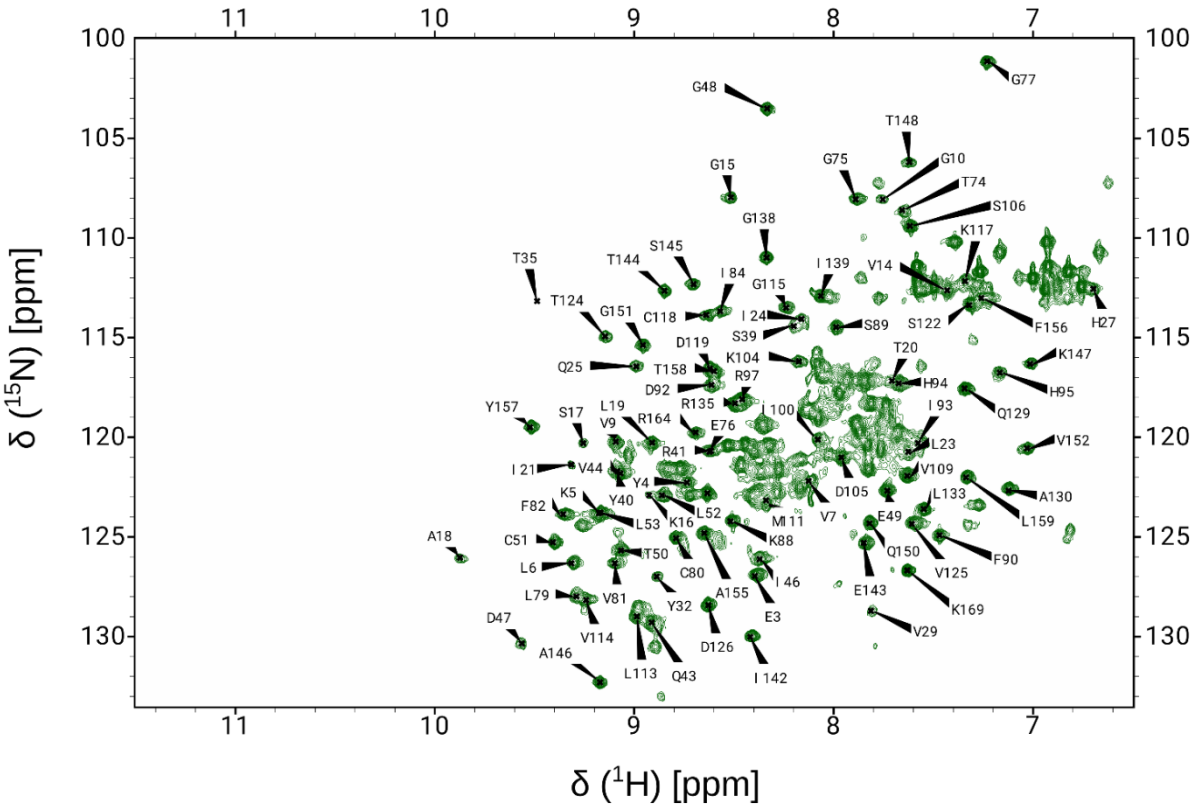

Figure S2 Assigned ^{1}H,^{15}N-HSQC spectrum of G12V K-Ras·Mg^{2+}·GTP. The assignments are shown partially with the full assignment deposited in BMRB, access number: 50773.

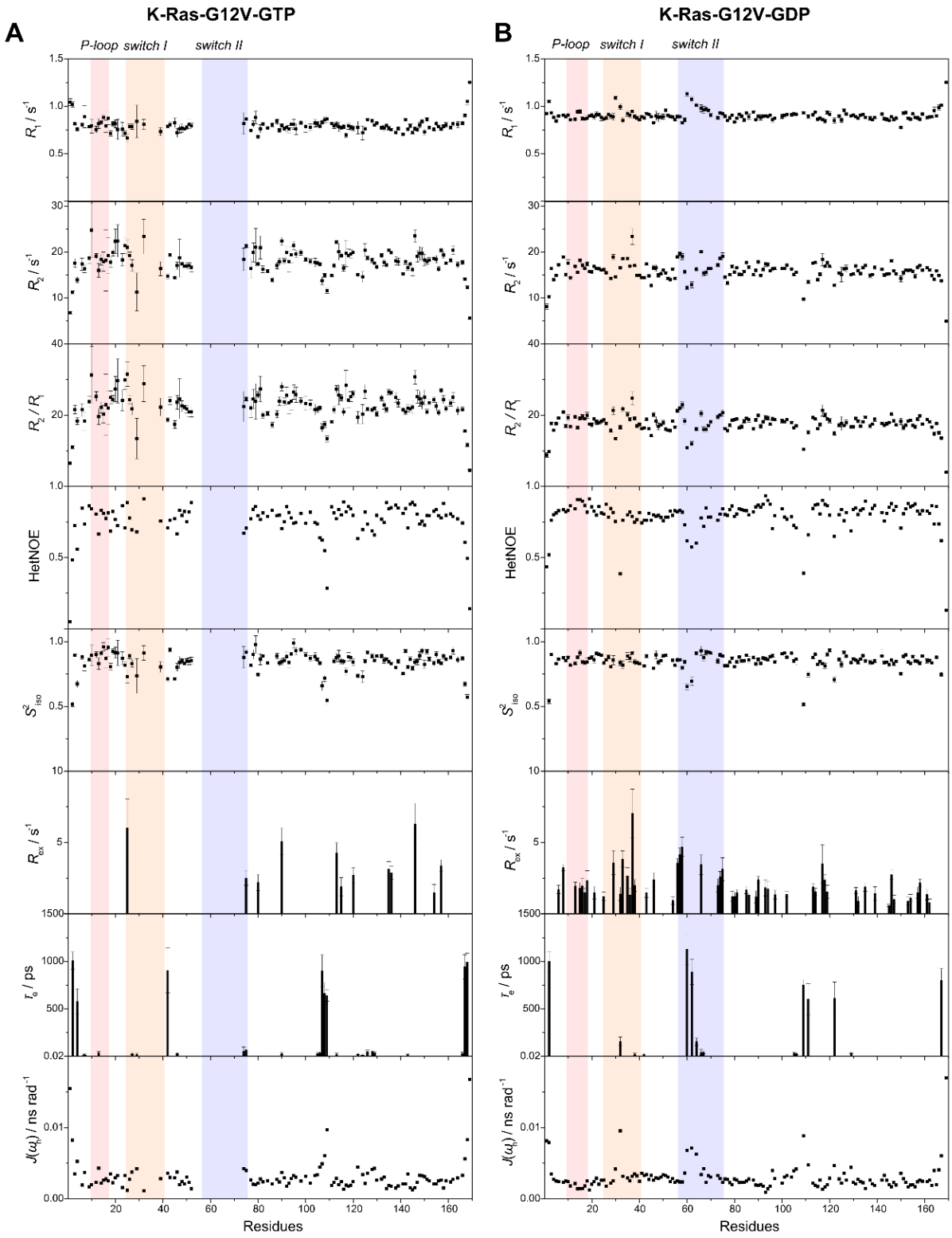

Figure S3 Relaxation data (R_1, R_2, ^{15}N-{^1H} HetNOE) and their analysis by Lipari-Szabo model-free formalism (S^2, R_{ex}, τ_e) and reduced spectral density mapping ($J(\omega_h)$) of G12V K-Ras in its (**A**) GTP- and (**B**) GDP-bound form as a function of the residue number. Regions of the P-loop (pink, residues 10-17), switch-I (orange, residues 25-40). and switch-II (blue, residues 57-75) are depicted.

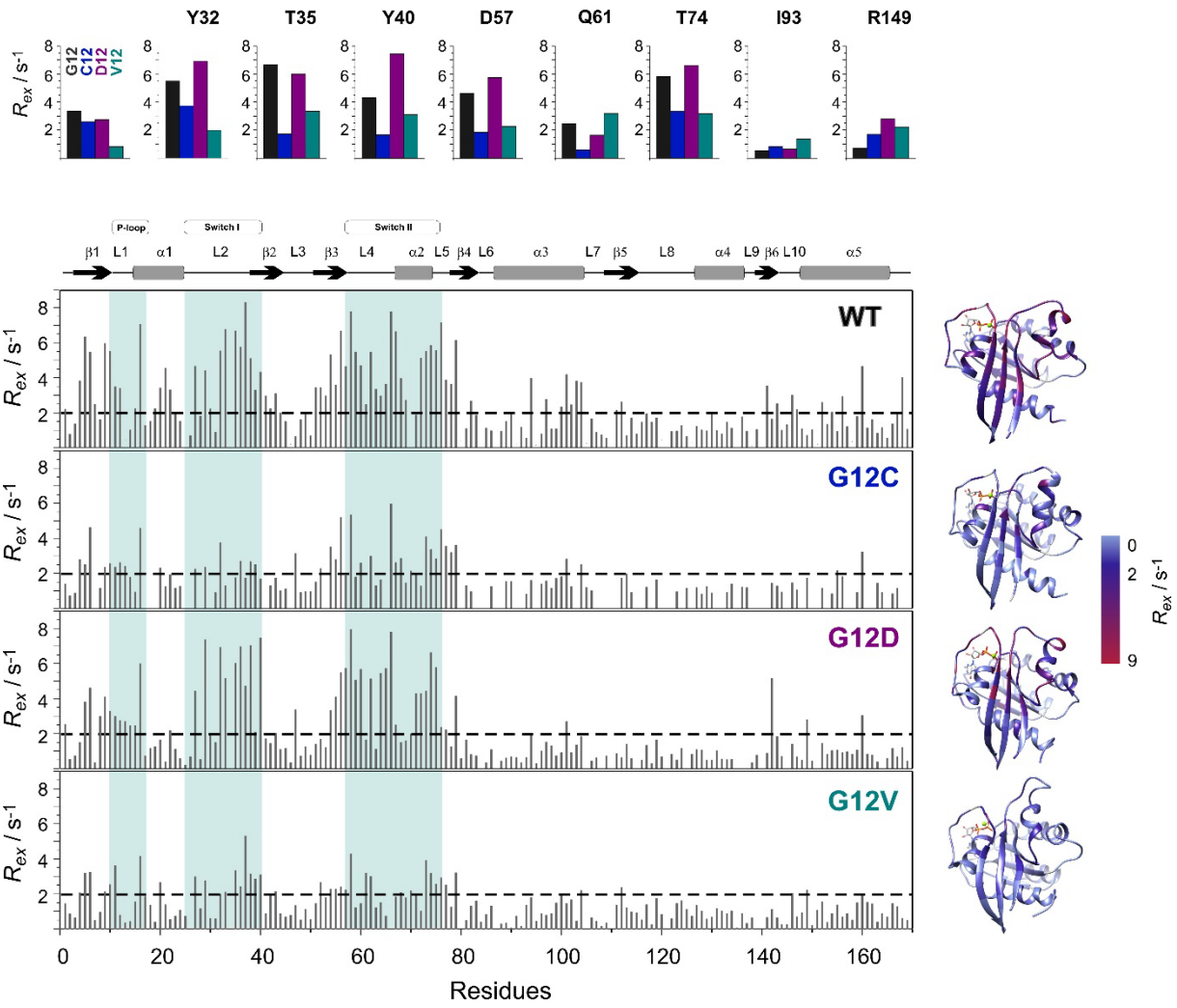

Figure S4 Values of ^{15}N R_{ex} (at 800 MHz for ^{1}H) of ^{15}N-labeled wild-type, G12C, G12D, and G12V K-Ras·Mg^{2+}·GDP complex at 25 °C (pH=7.4) as a function of amino acid sequence. R_{ex} is estimated from the difference in $R_{2,eff}$ at the lowest and highest ν_{CPMG} values. Secondary structural elements are indicated at the top. Regions of the P-loop, switch-I, and switch-II are highlighted in a blue background. For representative residues, ^{15}N R_{ex} in the investigated K-Ras variants are shown in large at the top. Values of R_{ex} are mapped on the ribbon diagram of the corresponding MD-derived structures ([2] and current study) on the right in a blue-to-red gradient.

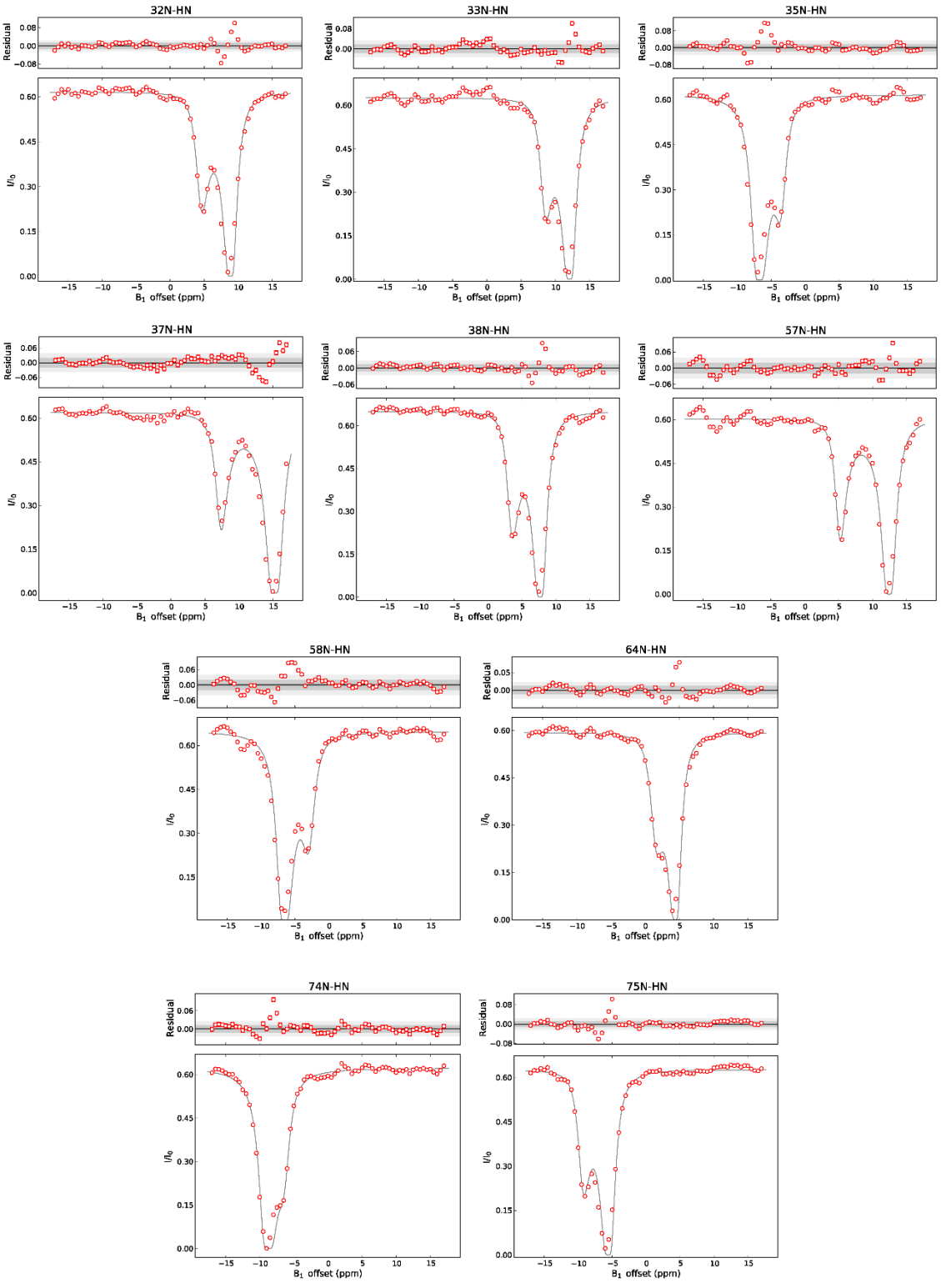

Figure S5 Plot of the fits of ^{15}N-CEST experiments of wt K-Ras·Mg^{2+}·GDP. Numerical results of the fits are shown in Table S5.

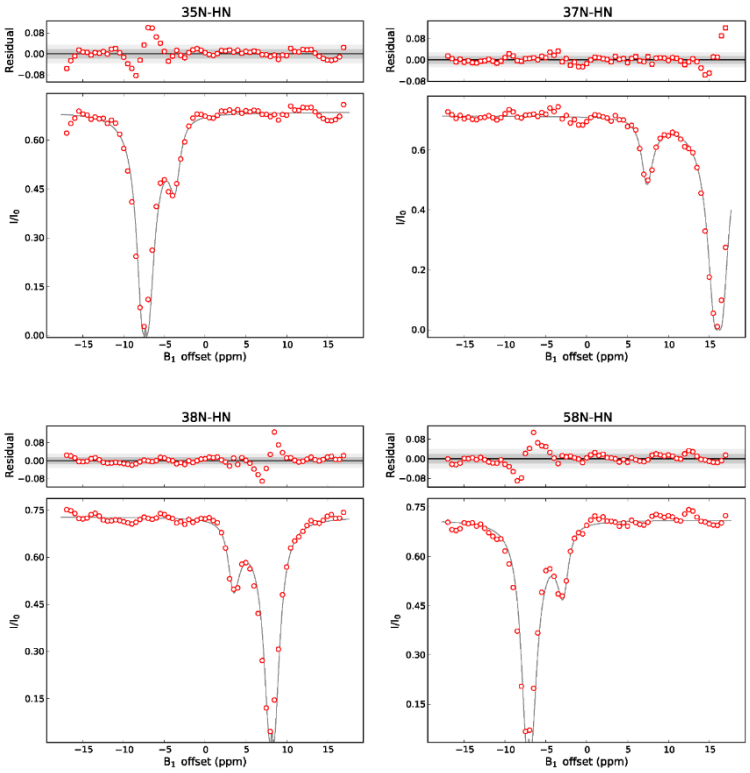

Figure S6 Plot of the fits of ^{15}N-CEST experiments of G12C K-Ras·Mg^{2+}·GDP. Numerical results of the fits are shown in Table S5.

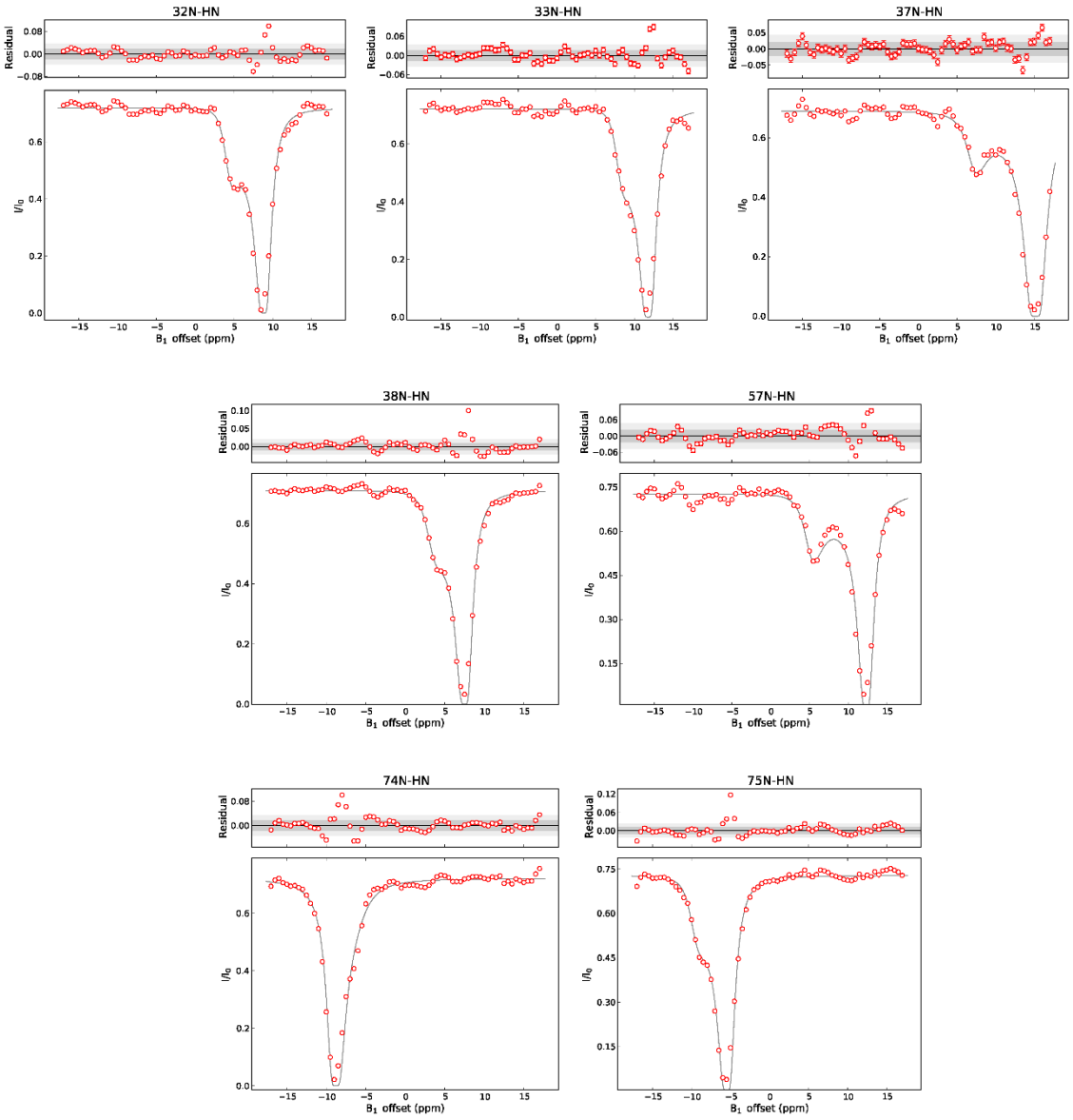

Figure S7 Plot of the fits of ^{15}N-CEST experiments of G12D K-Ras·Mg^{2+}·GDP. Numerical results of the fits are shown in Table S5.

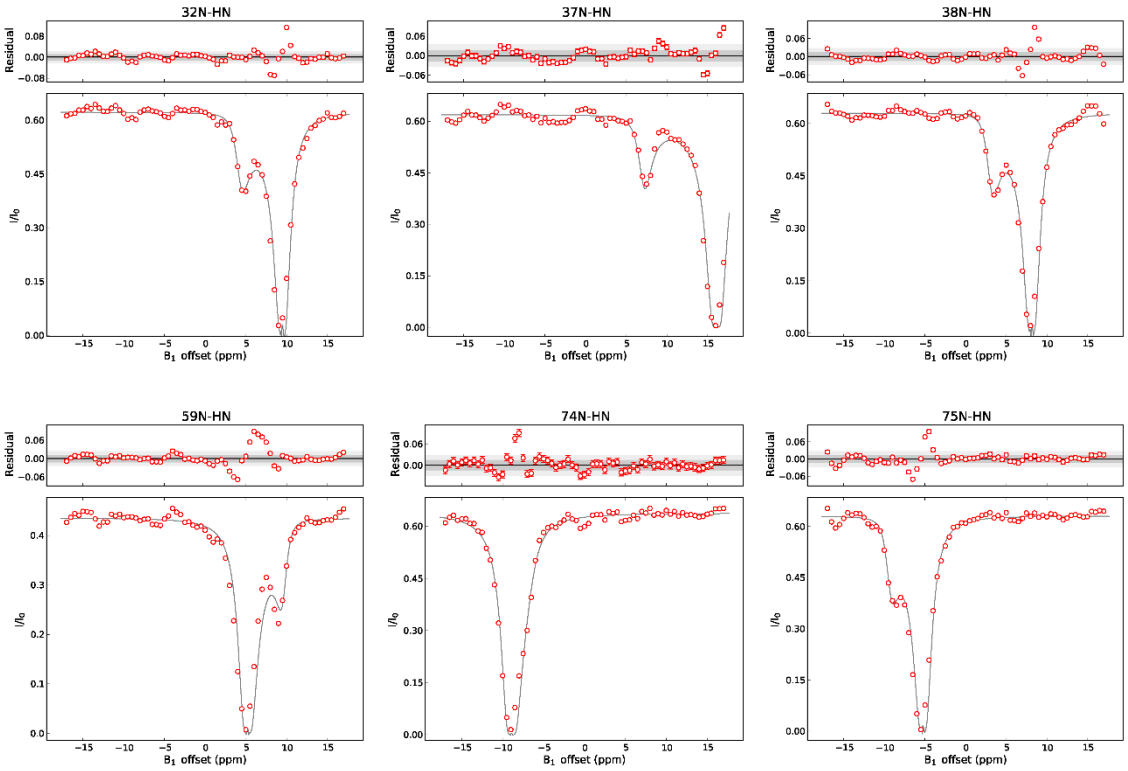

Figure S8 Plot of the fits of ^{15}N-CEST experiments of G12V K-Ras·Mg^{2+}·GDP. Numerical results of the fits are shown in Table S5.

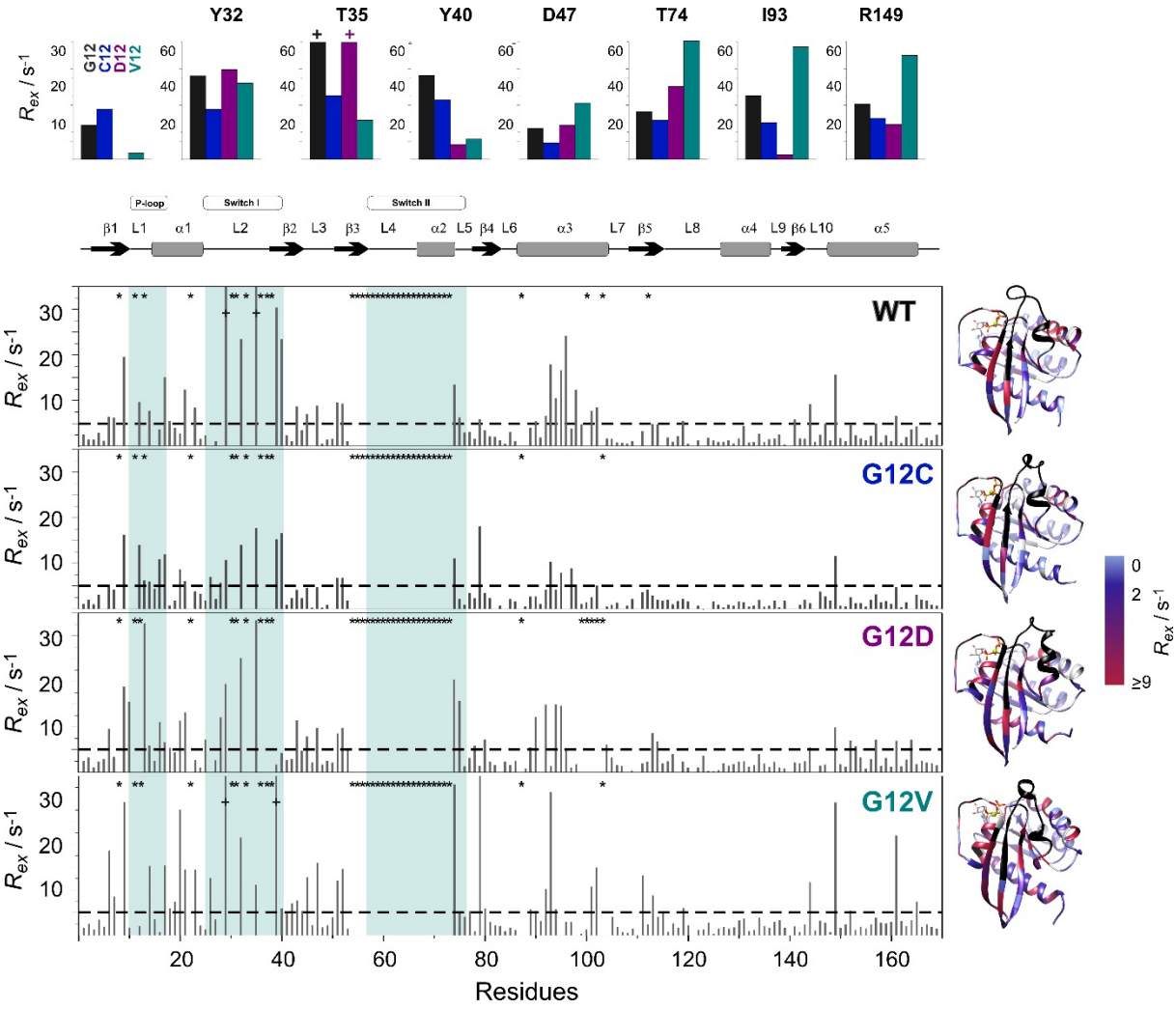

Figure S9 Values of ^{15}N R_{ex} (at 800 MHz for ^{1}H) of ^{15}N-labeled wild-type, G12C, G12D, and G12V K-Ras·Mg^{2+}·GTP complex at 25 °C (pH = 7.4) as a function of amino acid sequence. R_{ex} is estimated from the difference in $R_{2,eff}$ at the lowest and highest ν_{CPMG} values. Residues exhibiting R_{ex} > 35 s^{-1} (wt, G12V) are marked with a + sign. Secondary structural elements are indicated at the top. Regions of the P-loop, switch-I, and switch-II are highlighted in a blue background. Unassignable residues due to severe line broadening are marked with an asterisk. For representative residues, ^{15}N R_{ex} in the investigated K-Ras variants are shown in large at the top. Values of R_{ex} are mapped on the ribbon diagram of the corresponding MD-derived structures ([2] and current study) on the right in a blue-to-red gradient with unassignable residues due to line broadening are in black.

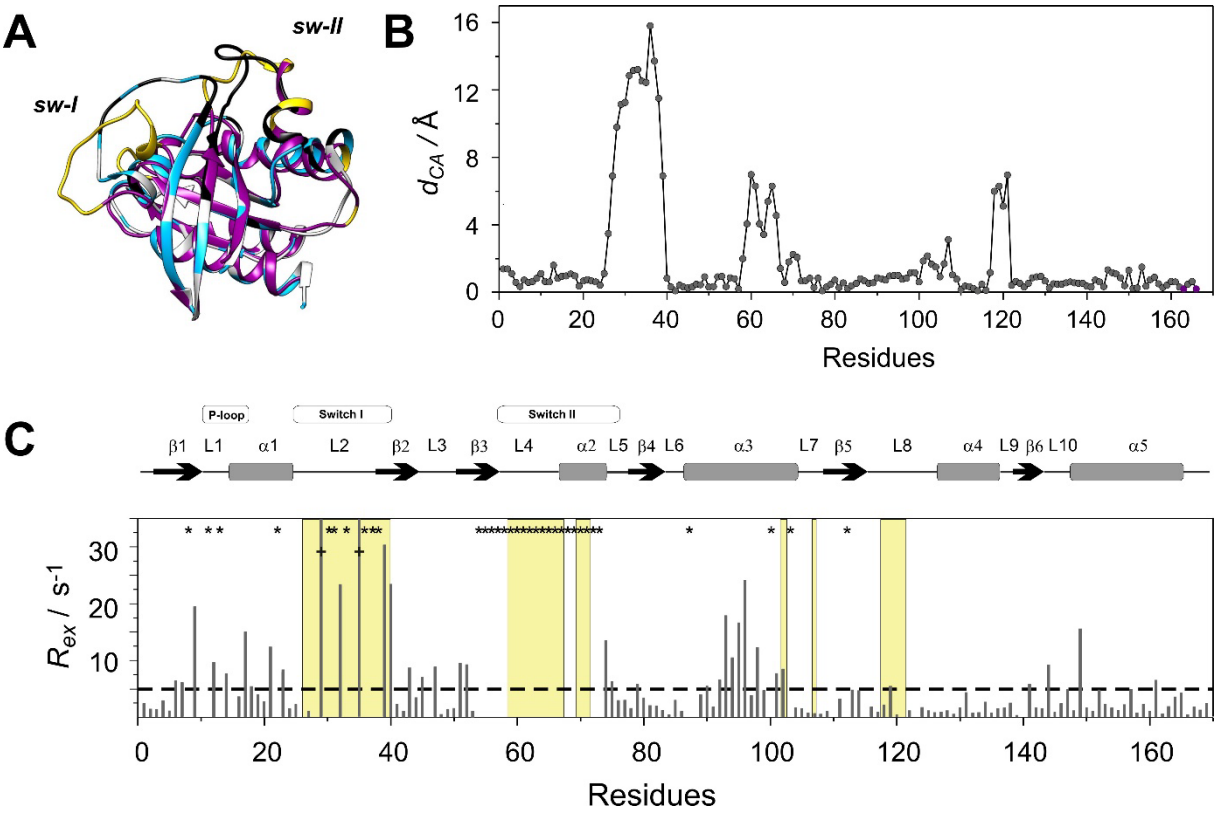

Figure S10 (**A**) Superimposed structures of K-Ras·Mg^{2+}·GTP (grey) and the nucleotide free H-Ras·Sos compex (PDB: 1BKD, magenta). Regions displaying C^{α} positional differences larger than 2 Å between the two complexes are highlighted in yellow. Residues exhibiting a contribution to transverse relaxation of R_{ex} > 2 Hz in K-Ras·Mg^{2+}·GTP are depicted in blue. (**B**) C^{α} positional differences between K-Ras·Mg^{2+}·GTP and H-Ras·Sos along the amino acid sequence. (**C**) Values of ^{15}N R_{ex} (at 800 MHz for ^{1}H) of ^{15}N-labeled wild-type K-Ras·Mg^{2+}·GTP (25 °C, pH=7.4) as a function of amino acid sequence. R_{ex} is estimated from the difference in $R_{2,eff}$ at the lowest and highest ν_{CPMG} values. Residues exhibiting R_{ex} > 35 s^{-1} are marked with a + sign. Unassignable residues due to severe line broadening are marked with an asterisk. Secondary structural elements are indicated at the top. Regions displaying d_{CA} > 2 Å in (**B**) are shown in a yellow background.

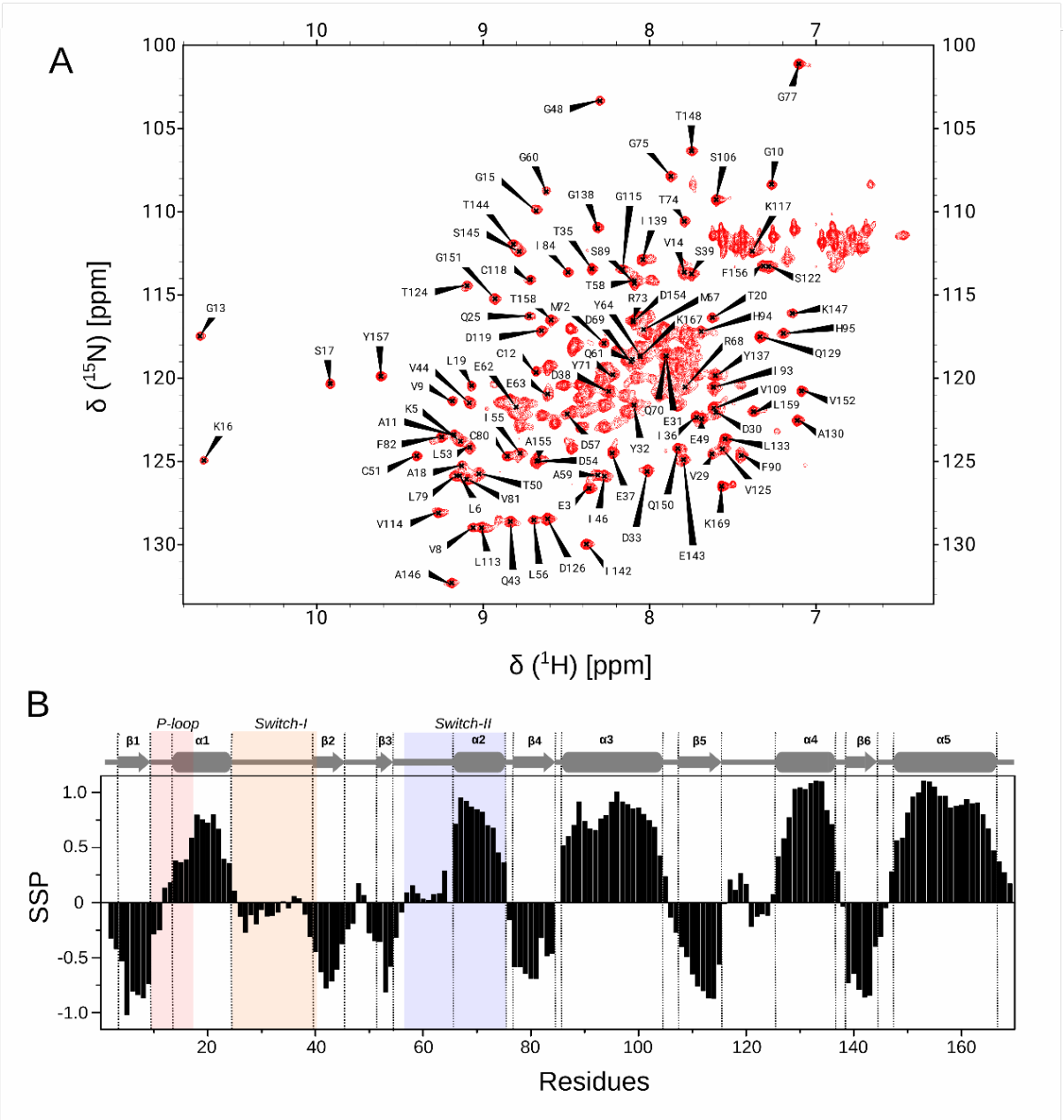

Figure S11 (**A**) Assigned ^{1}H,^{15}N-HSQC spectrum of Mg^{2+}-free G12C K-Ras·GDP. The assignments are shown partially, with the full assignment deposited in BMRB, access number: 50774. (**B**) Secondary structure propensities (SSP) of Mg^{2+}-free G12C K-Ras. Secondary structure elements are drawn at the top. Regions of the P-loop (light red, residues 10-17), switch-I (orange, residues 25-40), and switch-II (light blue, residues 57-75) are highlighted.

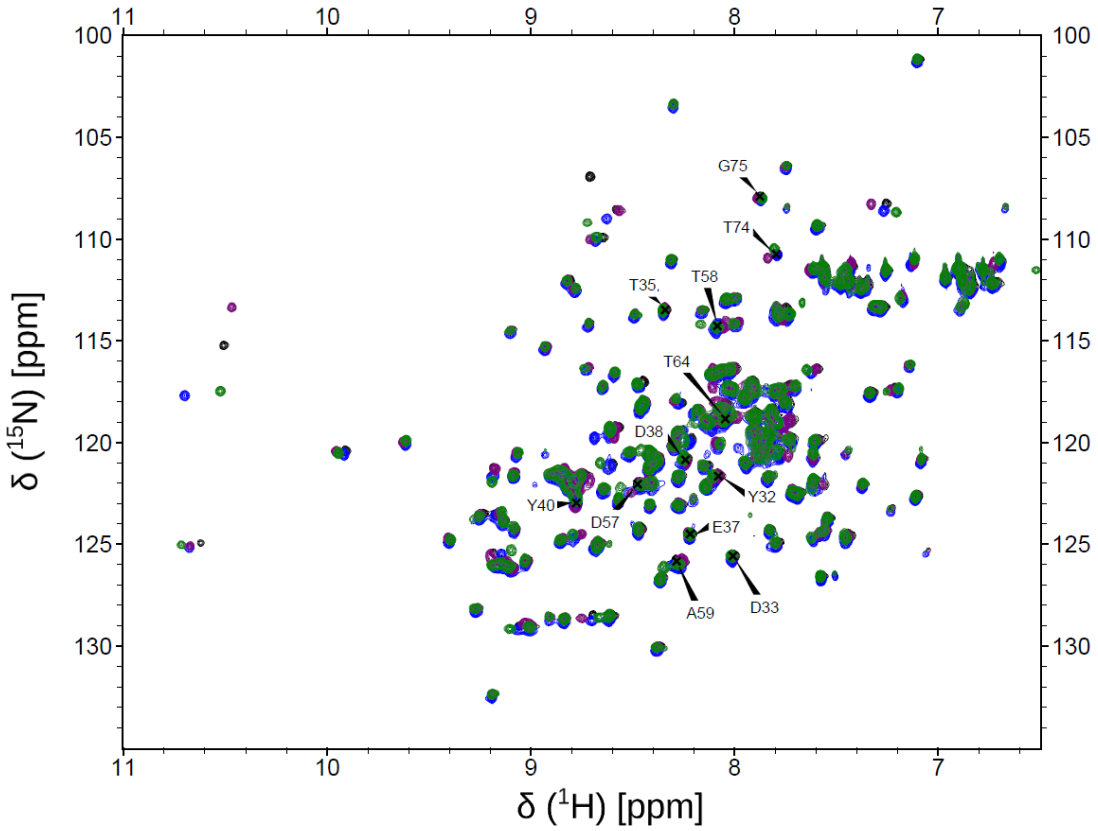

Figure S12 Overlaid ^{1}H,^{15}N-HSQC spectra of GDP-bound Mg^{2+}-free wt (black), G12C (blue), G12D (pruple), and G12V (green) K-Ras. The assignment of the CEST-active residues are shown.

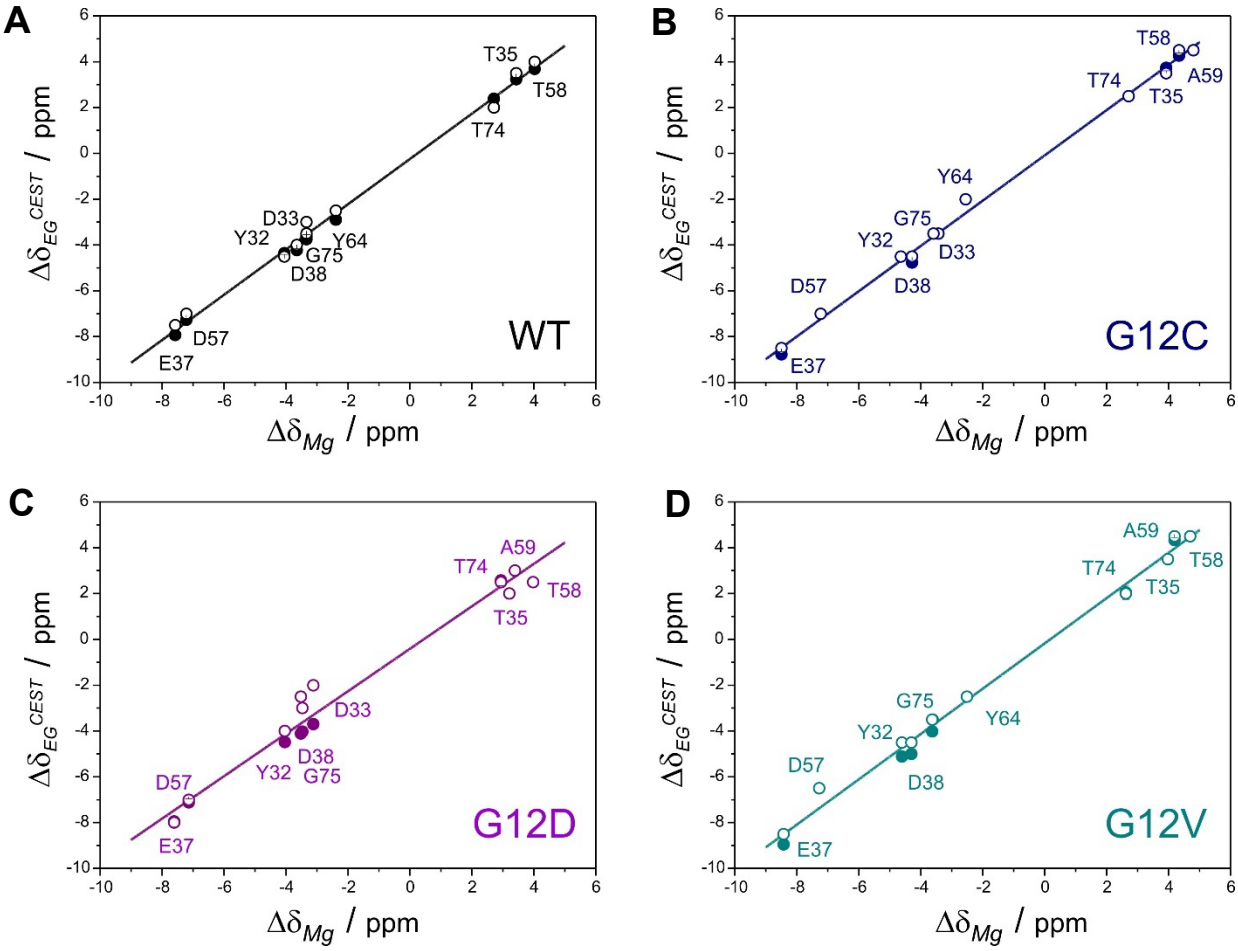

Figure S13 Correlation between ^{15}N backbone chemical shift differences derived from CEST measurements ($\Delta\delta_{EG}^{CEST}$) and those detected between the Mg^{2+}-bound and Mg^{2+}-free forms ($\Delta\delta_{Mg}$) in **(A)** wt, **(B)** G12C, **(C)** G12D, and **(D)** G12V K-Ras·GDP. Fitted and estimated (based on the difference between the two minima of the CEST-curve) values of $|\Delta\delta_{EG}|$ are depicted in closed and empty circles, respectively.

.

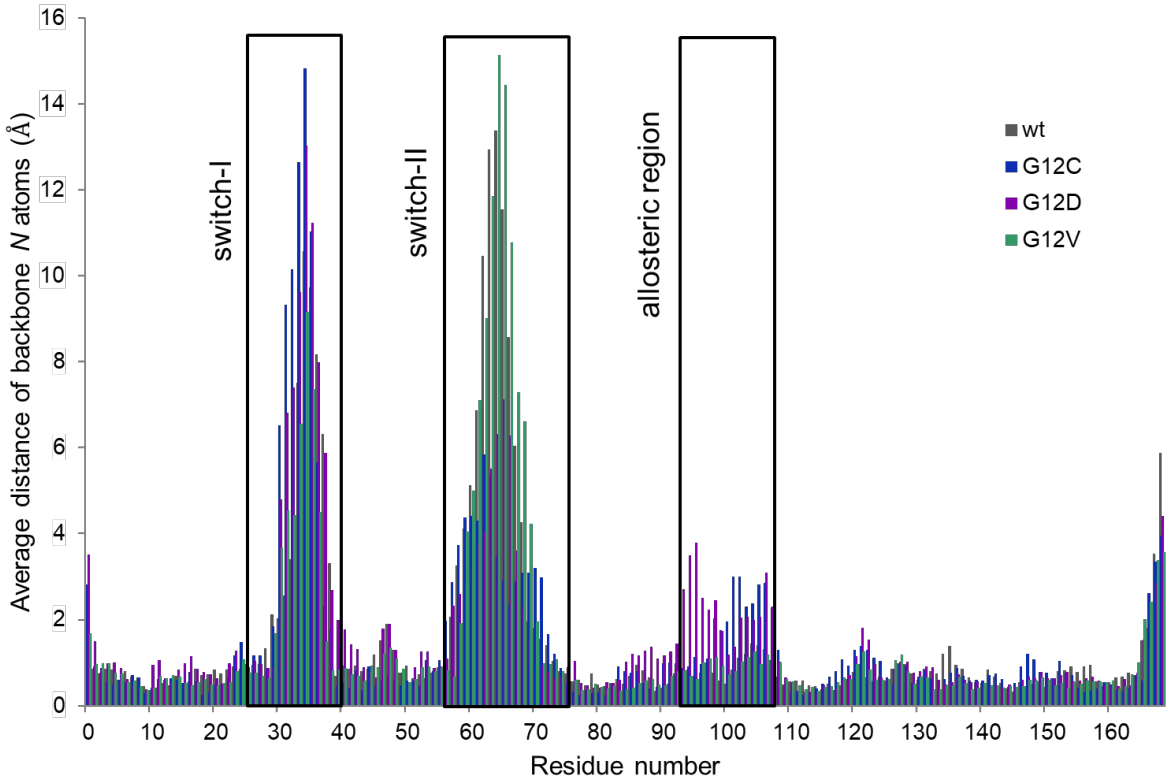

Figure S14 Average deviation (in Å) of backbone amide *N* atoms between the GDP-bound Mg^{2+}-loaded and Mg^{2+}-free forms by MD simulations along the sequence for K-Ras-wt (black), G12C (blue), G12D (purple), and G12V (green) variants.

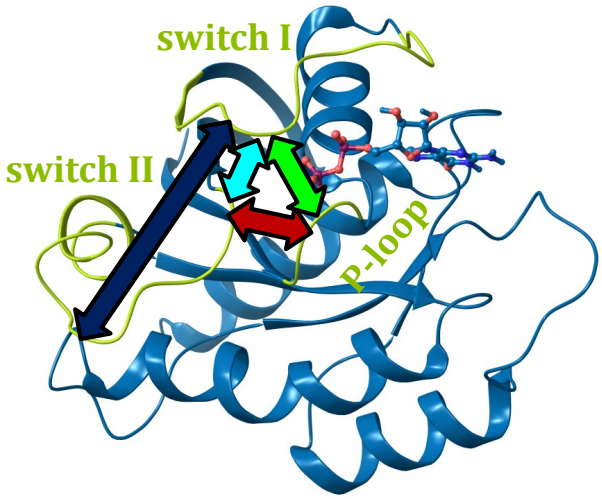

P-loop ↔ switch II (proximal)
P-loop ↔ switch I
switch-I ↔ switch-II (proximal)
switch-I ↔ switch-II (distant)

C^{α}- C^{α} distance (Å)	wt + Mg^{2+}	G12C + Mg^{2+}	G12D + Mg^{2+}	G12V + Mg^{2+}	WT no Mg^{2+}	G12C no Mg^{2+}	G12D no Mg^{2+}	G12V no Mg^{2+}	GEF-complex (no Mg^{2+}, no GDP) ***crystal structure***
X12-A59	7.1±0.5	6.8±0.5	7.9±0.6	7.2±0.5	6.2±0.4	6.1±0.3	7.5±0.3	5.9±0.3	7.1
X12-G60	7.3±1.2	4.5±0.5	7.5±1.1	5.3±0.9	9.4±0.4	8.8±0.3	4.1±0.3	9.4±0.4	7.6
X12-Q61	8.1±1.1	7.1±0.8	8.3±1.4	8.4±1.4	12.1±1.0	10.2±0.4	5.5±0.5	11.1±0.8	8.3
X12-P34	7.4±0.6	6.9±0.7	9.3±1.2	9.3±0.8	14.6±0.8	18.7±0.8	17.4±0.9	15.9±1.1	18.8
X12-T35	9.0±0.6	8.8±0.5	11.3±1.5	11.2±0.7	18.4±0.8	20.6±0.7	20.7±0.9	19.1±1.0	21.0
T35-A59	5.4±0.5	5.6±0.7	5.9±1.2	6.2±0.8	17.0±0.8	20.4±0.6	17.6±1.1	17.6±0.9	14.4
T35-G60	7.2±1.0	7.8±0.8	8.6±1.2	9.2±0.9	18.9±1.0	22.7±0.7	19.9±1.0	19.3±0.9	14.8
T35-Q61	10.2±0.9	10.1±1.3	8.9±1.9	10.0±1.3	18.3±1.3	26.5±0.7	21.3±1.2	18.2±1.4	16.1
T35-E63	16.1±1.0	14.0±1.8	15.1±1.8	13.8±1.2	16.9±2.1	30.7±0.8	23.3±1.3	15.8±2.4	21.4
T35-Y64	17.4±1.0	14.6±1.3	17.1±1.4	15.7±1.1	15.9±1.4	29.1±0.9	22.6±1.4	13.6±2.7	20.8

Figure S15 Loosening of the overall structure of K-Ras proteins upon Mg^{2+} release – seen in the MD simulations. The table shows the distance of the C^{α} atoms of selected residue-pairs in the MD simulations and in the crystal structure of the GEF-bound nucleotide- and Mg^{2+}-free wt H-Ras (PDB code: 1XD2[4]).

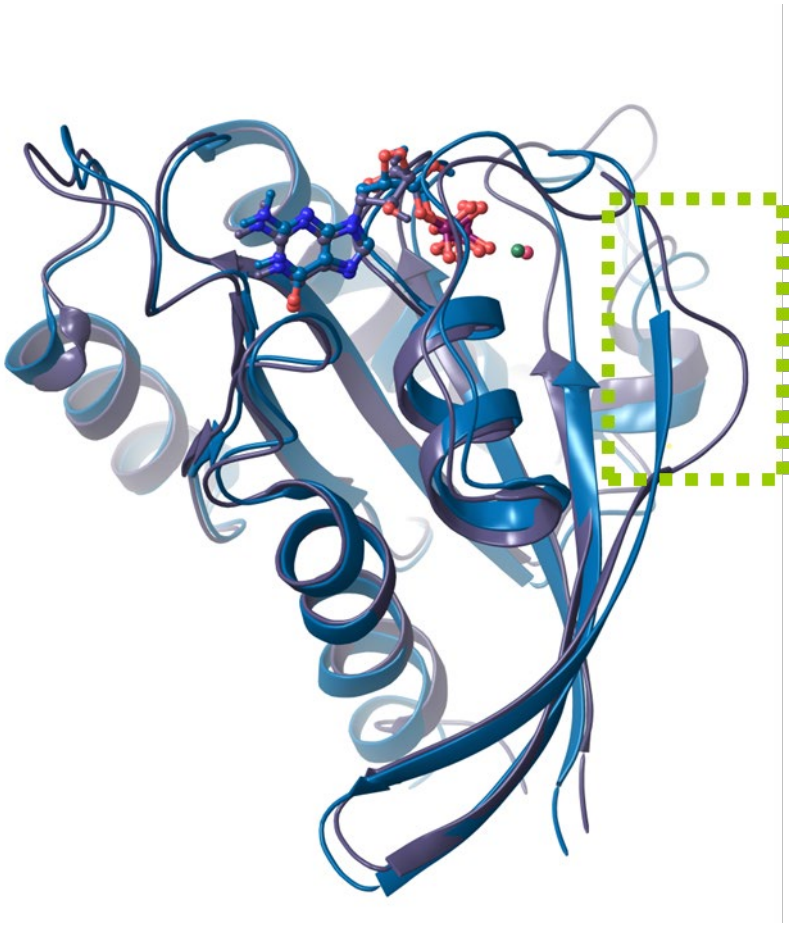

C^{α}- C^{α} distance (Å)	wt	G12C	G12D	G12V	wt no Mg^{2+}	G12C no Mg^{2+}	G12D no Mg^{2+}	G12V no Mg^{2+}	GEF-complex (no Mg^{2+}, no GDP) ***crystal structure***
I36-A59	6.2±0.5	6.5±0.7	6.1±0.5	8.6±0.7	16.2±0.7	17.5±0.5	16.0±1.0	16.1±1.1	16.6
E37-T58	4.7±0.4	5.2±0.3	4.7±0.5	10.4±1.1	12.9±0.8	11.1±0.4	13.2±1.7	13.1±0.8	15.2
D38-D57	5.2±0.3	5.2±0.2	5.2±0.2	9.9±0.5	9.7±0.5	7.2±0.3	10.1±0.8	10.0±0.7	12.2
***H* bonds**	9.6	9.3	9.7	7.9	7.9	8.1	7.4	7.8	7

Figure S16 Shortening of the β2/β3 strands – as seen in the MD simulations. In the MD-derived average structure, GDP-bound KRas-wt is blue, while G12V is purple. The shortened β2/β3 strands are shown in the light green rectangle. The table shows the distance of C^{α} atoms of the 3 outermost *H*-bonding residue pairs between β2 and β3, and the total number of *H*-bonds formed between the two strands in the simulations.

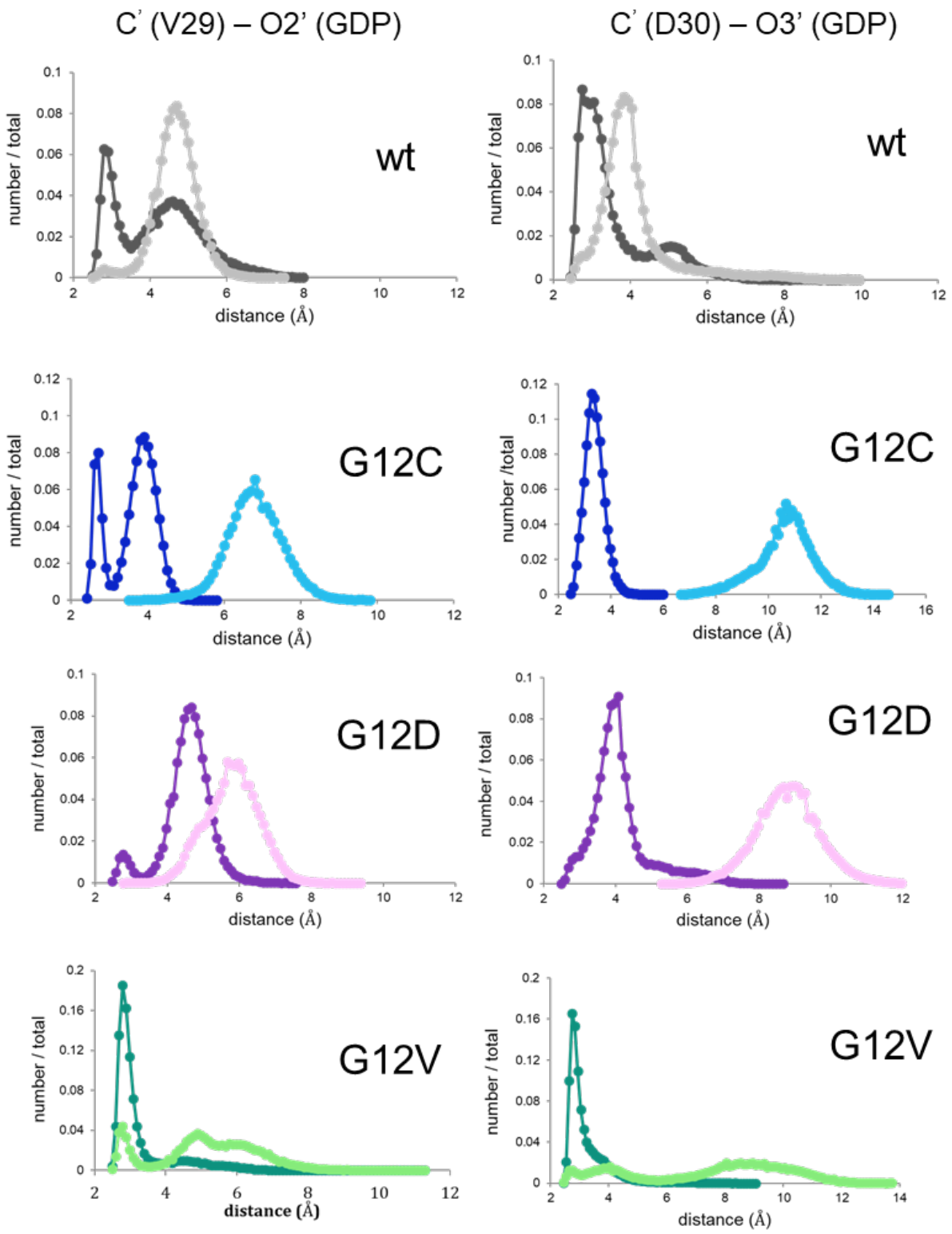

Figure S17 Weakened association between the sugar ring of GDP and the V29 and D30 residues of switch-I as seen in the MD simulations of GDP-bound K-Ras-wt (grey), G12C (blue), G12D (purple), G12V (green) in the Mg^{2+}-bound (dark colors) and Mg^{2+}-free states (light colors). The distribution of the distances between O2' (in case of V29) and O3' (in case of D30) of the GDP and C' (carbonyl) of the residue are shown for each simulation.

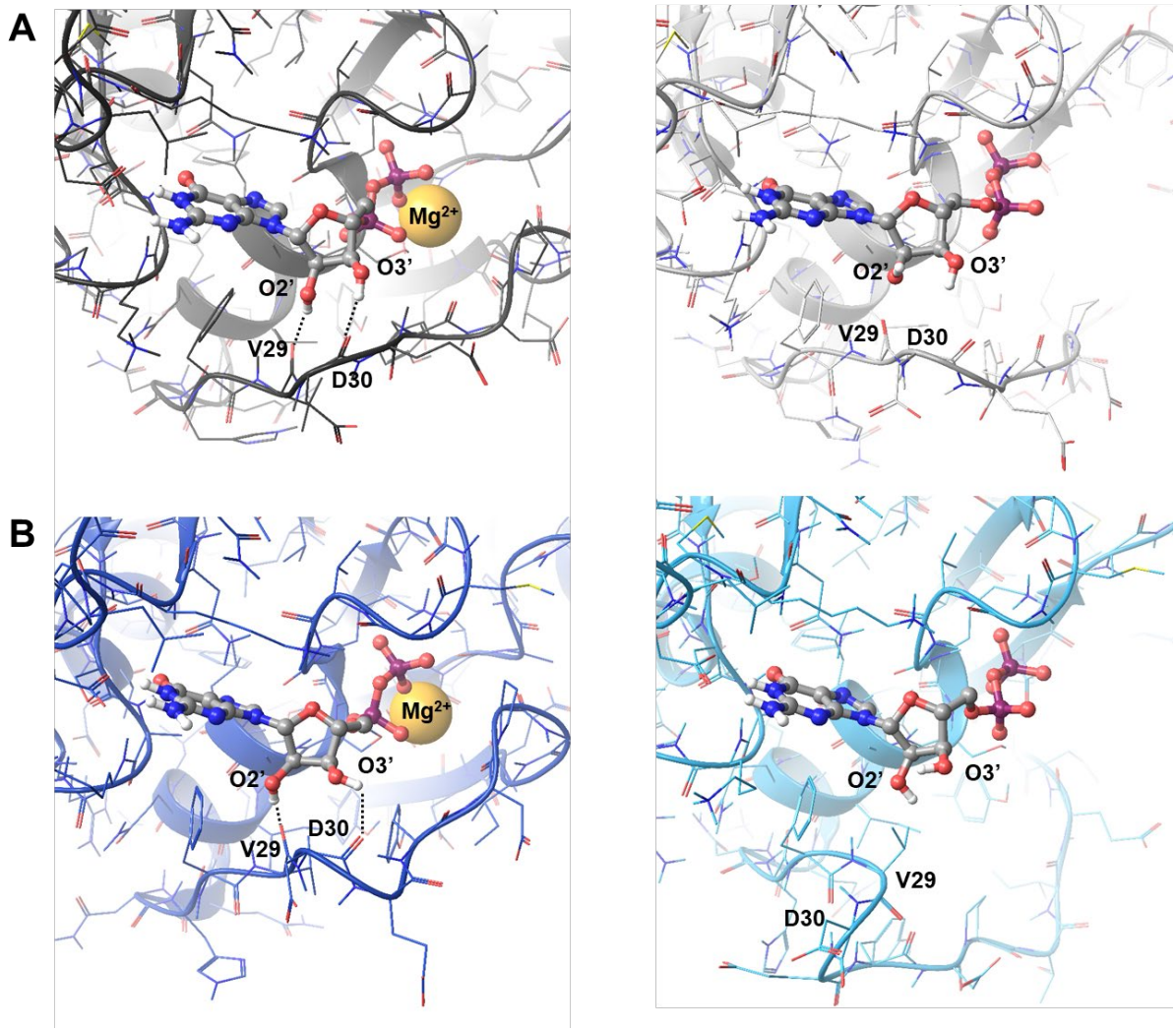

Figure S18 Two examples for the changes illustrated on Figure S17. **(A)** In case of GDP-bound K-Ras-wt moderate changes are caused by Mg^{2+} loss in the interaction between the sugar ring of GDP and switch-I (Mg^{2+}-bound and Mg^{2+}-free form are shown in dark grey and light grey, respectively), while **(B)** in case of the GDP-bound G12C variant the changes are more striking (Mg^{2+}-bound and Mg^{2+}-free form are shown in dark blue and light blue, respectively). Each simulation is represented by the mid-structures of the most populated cluster.

References

[1] G. Pálfy, I. Vida, A. Perczel, *Biomol. NMR Assign.* **2020**, *14(1)*, 1-7.

[2] D. K. Menyhárd, G. Pálfy, Z. Orgován, I. Vida, G. M. Keserű, A. Perczel, *Chem. Sci.* **2020**, *11*, 9272-9289

[3] Y. Ito, K. Yamasaki, J. Iwahara, T. Terada, A. Kamiya, M. Shirouzu, Y. Muto, G. Kawai, S. Yokoyama, E. D. Laue, M. Wälchli, T. Shibata, S. Nishimura, T. Miyazawa, *Biochemistry* **1997**, *36(30)*, 9109-9119

[4] H. Sondermann, S. M. Soisson, S. Boykevisch, S. S. Yang, D. Bar-Sagi, J. Kuriyan, *Cell* (**2004**) *119*, 393-405